DETERMINATION OF BIOMARKERS FOR MILD COGNITIVE IMPAIRMENT IN PARKINSON'S DISEASE USING MAGNETIC RESONANCE SPECTROSCOPIC IMAGING

by

Sevim Cengiz

B.Sc., Biomedical Engineering, Erciyes University, 2013

Submitted to the Institute of Biomedical Engineering
in partial fulfillment of the requirements
for the degree of
Master of Science
in
Biomedical Engineering

Boğaziçi University
2016

DETERMINATION OF BIOMARKERS FOR MILD COGNITIVE IMPAIRMENT IN PARKINSON'S DISEASE USING MAGNETIC RESONANCE SPECTROSCOPIC IMAGING

APPROVED BY:

Assist. Prof. Dr. Esin Öztürk Işık .....
(Thesis Advisor)

Assoc. Prof. Dr. Bora Garipcan .....

Prof. Dr. Tamer Demiralp .....

DATE OF APPROVAL: 25 July 2016

ACKNOWLEDGEMENTS

This study would not have been possible without the help of my advisor, Assist. Prof. Dr. Esin Öztürk Işık, in many ways. I would like to thank Dr. Işık for all the help and advice, for all the patience, and for giving me this opportunity to study on determination of biomarkers for mild cognitive impairment in Parkinson's disease using magnetic resonance spectroscopic imaging, which also helped me in doing lots of research that let me improve myself, gain knowledge, and widen my horizons. Moreover, I would like to thank my thesis committee Prof. Dr. Tamer Demiralp and Assoc. Prof. Dr. Bora Garipcan for their encouraging comments.

I would like to thank my colleagues, Dilek Betül Arslan, Gökçe Hale Hatay, Ani Kıçik, and Emel Erdoğdu for their help and advice on my study. I am also thankful to my parents and lovely spouse, Ilter, for all the support they gave me during this period.

This study was supported by TÜBİTAK project #115S219, Bogazici University BAP 10844SUP grant, and the Ministry of Development project #2010K120330.

ACADEMIC ETHICS AND INTEGRITY STATEMENT

I, Sevim Cengiz, hereby certify that I am aware of the Academic Ethics and Integrity Policy issued by the Council of Higher Education (YÖK) and I fully acknowledge all the consequences due to its violation by plagiarism or any other way.

Name :

Signature:

Date:

ABSTRACT

DETERMINATION OF BIOMARKERS FOR MILD COGNITIVE IMPAIRMENT IN PARKINSON'S DISEASE USING MAGNETIC RESONANCE SPECTROSCOPIC IMAGING

Parkinson's disease (PD) patients could be categorized as PD with cognitively normal (PD-CN), PD with mild cognitive impairment (PD-MCI), and PD with dementia (PDD). There is a need for finding noninvasive biomarkers for the early diagnosis of PD-MCI. Proton magnetic resonance spectroscopic imaging (^{1}H-MRSI) is a non-invasive MR technique that provides spectroscopic information about metabolic activity of the brain. 19 patients with PD-MCI and 21 patients with PD-CN were included in this study and neuropsychological tests were performed. Multi-voxel ^{1}H-MRSI data were acquired in all patients. An MRSI data analysis tool was developed to create ^{1}H MR spectroscopic peak parameter maps out of raw MRSI data and overlay them onto reference T2-weighted MR images. FMRIB Software Library (FSL) tool was used to register metabolite maps overlaid onto T2-weighted MR images to an MNI152 brain atlas. A Mann-Whitney rank-sum test was applied to compare the differences of metabolic parameters and neuropsychological test scores between PD-MCI and PD-CN. A Friedman test was used to analyze the MR spectroscopic metabolite ratio variations in different brain regions of PD-MCI and PD-CN. Spearman rank correlation coefficient was used to find correlations of neuropsychological test scores and MRS metabolite ratios. There were no significant differences in MRS metabolite ratios in different brain regions of PD-MCI and PD-CN after accounting for multiple comparisons. However, frontal lobe and cerebral white matter showed trends for metabolic differences. Neuropsychological test scores were correlated with several spectroscopic parameters. The results of this study might enable a definition of a biomarker for PD-MCI diagnosis in the future, when combined with possible other MR based biomarkers.

Keywords: Parkinson's disease, mild cognitive impairment, registration, multi-voxel, proton magnetic resonance spectroscopic imaging.

ÖZET

MANYETİK REZONANS SPEKTROSKOPİK GÖRÜNTÜLEME KULLANARAK HAFİF KOGNİTİF BOZUKLUĞU OLAN PARKİNSON HASTALARINDA BİYOİŞARETLECİYİLERİN BELİRLENMESİ

Parkinson hastalığı (PH), PH işlevsel normal (PH-KN), PH hafif kognitif bozukluk (PH-HKB) ve PH demans (PHD) olarak sınıflandırılabilmektedir. PH-HKB erken tanısı için noninvazif biyoişaretleyiciler bulmaya ihtiyaç vardır. Proton manyetik rezonans spektroskopik görüntüleme (^{1}H-MRSG), beyindeki metabolik aktivite hakkında spektroskopik bilgi sağlayan bir noninvazif MR tekniğidir. 19 PH-HKB ve 21 PH-KN hastaları bu çalışmaya dahil edildi ve nöropsikolojik testler uygulandı. Tüm hastalarda çoklu voksel ^{1}H-MRSG verileri alındı. İşlenmemiş MRSG verilerinden çıkarılan ^{1}H MR spektroskopik pik parametre haritaları yaratmak ve onları referans T2-ağırlıklı MR görüntüler üzerine yerleştirmek için bir MRSG veri analiz aracı geliştirildi. T2-ağırlıklı görüntüler üzerine yerleştirilen metabolik haritaları bir MNI152 beyin haritasına çakıştırmak için FMRIB yazılım aracı (FSL) kullanıldı. Mann-Whitney sıra toplam testi uygulanarak, PH-HKB ve PH-KN hastalarının metabolik parametreleri ve nöropsikolojik test skorları arasındaki farklar karşılaştırıldı. Friedman testi ile PH-HKB ve PH-KN hastalarında, farklı beyin bölgelerindeki MR spektroskopik metabolit oranların değişimleri incelendi. Nöropsikolojik test skorlarının MR spektroskopik metabolit oranları ile korelasyonlarına Spearman sıra korelasyon katsayısı kullanılarak bakıldı. Çoklu karşılaştırmaları hesaba katınca, PH-HKB ve PH-KN'nın farklı beyin bölgelerinde MRS metabolitlerinde anlamlı farklılıklar yoktu. Buna rağmen, frontal lob ve serebral beyaz maddede metabolit farklılıklara dair bir eğilim görüldü. Nöropsikolojik test skorları ve pek çok spektroskopik parametreler arasında bir korelasyon vardı. Bu çalışmanın sonuçları, ileride başka olası MR temelli biyoişaretleyiciler ile birleştirilerek, PH-HKB tanısı için bir biyoişaretleyici tanımlanmasında kullanılabilir.

Anahtar Sözcükler: Parkinson hastalığı, hafif kognitif bozukluk, imge çakıştırma, çoklu voksel, proton manyetik rezonans spektroskopik görüntüleme

TABLE OF CONTENTS

ACKNOWLEDGEMENTS . . . iii
ACADEMIC ETHICS AND INTEGRITY STATEMENT . . . iv
ABSTRACT . . . v
ÖZET . . . vi
LIST OF FIGURES . . . ix
LIST OF TABLES . . . x
LIST OF SYMBOLS . . . xi
LIST OF ABBREVIATIONS . . . xii
1. INTRODUCTION . . . 1
1.1 The Principles of Magnetic Resonance Imaging . . . 1
1.1.1 Analysis Tools for Magnetic Resonance Imaging . . . 2
1.1.1.1 Brain Extraction (BET) . . . 3
1.1.1.2 Image Registration . . . 3
1.2 The Principles of Magnetic Resonance Spectroscopy . . . 5
1.2.1 Magnetic Resonance Spectroscopic Imaging . . . 6
1.2.1.1 MR Spectroscopic Imaging Data Acquisition . . . 7
1.2.1.2 MR Spectroscopic Imaging Data Processing Software . 9
1.2.2 Diseases and Diagnosis in ^{1}H-MRSI . . . 10
1.2.3 Metabolites in ^{1}H-MRSI . . . 11
1.2.3.1 Alanine(Ala) . . . 11
1.2.3.2 Aspartate (Asp) . . . 11
1.2.3.3 γ-Aminobutyric acid (GABA) . . . 11
1.2.3.4 Creatine (Cr) and Phosphocreatine (PCr) . . . 12
1.2.3.5 Compounds Containing Choline (tCho) . . . 12
1.2.3.6 Glucose(Glc) . . . 13
1.2.3.7 Glutamate (Glu) . . . 13
1.2.3.8 Glutamine (Gln) . . . 13
1.2.3.9 Glutathione (GSH) . . . 14
1.2.3.10 Glycine (Gly) . . . 14

1.2.3.11 Lactate (Lac) . . . 14
1.2.3.12 Myo-inositol (mI) . . . 15
1.2.3.13 N-Acetylaspartate & N-Acetylaspartylgluatamate . . . 15
1.2.3.14 Scyllo-inositol (sI or s-Ins) . . . 15
1.2.3.15 Taurine (Tau) . . . 16
1.3 What is Parkinson's Disease? . . . 16
1.3.1 Diagnosis of Parkinson's Disease . . . 17
1.4 Assessment of MRS Findings in PD-CI, PD-MCI, and PDD . . . 19
1.5 The Objective of the Study . . . 20
2. MATERIALS and METHODS . . . 22
2.1 Subjects . . . 22
2.2 Diagnostic Assessment . . . 23
2.3 Data Acquisition MR Protocol . . . 23
2.4 Post Processing . . . 24
2.4.1 Registration of Metabolite Maps Overlaid onto Reference T2-weighted MR Image to MNI 152 Atlas . . . 30
2.5 Region of Interest Analysis . . . 33
2.6 Statistical Analysis . . . 33
3. RESULTS . . . 34
3.1 Demographics and Neuropsychological Assessments . . . 34
3.2 MRSI Markers . . . 34
3.3 Pairwise Correlation . . . 36
3.4 Spatial Distribution of ^{1}H-MRSI . . . 38
4. DISCUSSION . . . 43
5. CONCLUSION . . . 46
APPENDIX A. Software Packages . . . 47
REFERENCES . . . 48

LIST OF FIGURES

Figure 1.1	A brain extraction example of a T2-weighted MR image.	3
Figure 1.2	An example of T2-weighed image registered to MNI152 brain atlas.	4
Figure 1.3	PRESS sequence diagram.	7
Figure 1.4	STEAM sequence diagram.	8
Figure 2.1	The sagittal view of two different regions of interest in an example patient.	24
Figure 2.2	Example LCModel outputs.	25
Figure 2.3	Image space for Philips MRSI data.	26
Figure 2.4	NAA+NAAG/Cr+PCr peak parameter maps that belongs to 3 slices.	26
Figure 2.5	Voxel marked in yellow circle shows anterior cingulate.	27
Figure 2.6	Sagittal and axial MNI152 brain atlas with the corresponding voxel marked in yellow.	27
Figure 2.7	Example selection of a voxel in a metabolite map.	28
Figure 2.8	Metabolite map overlaid onto reference T2-weighted image.	29
Figure 2.9	The GUI of the data analysis tool.	30
Figure 2.10	a. raw T2-weighted image b. MNI 152 brain atlas c. registered T2-weighted image to MNI 152 brain atlas (coronal, sagittal, and axial).	31
Figure 2.11	MRSI registration steps.	32

LIST OF TABLES

Table 2.1	The demographic information of the subjects included in this study.	22
Table 2.2	MR Acquisition parameters for T2-weighted MR image and ^{1}H-MRSI.	24
Table 3.1	Neuropsychological test scores of all patients.	35
Table 3.2	Comparisons of the neuropsychological test scores.	36
Table 3.3	Comparisons of different metabolite ratios in different brain regions.	37
Table 3.4	Spearman's correlation between metabolite ratios and neuropsychological test scores for PD-CN.	40
Table 3.5	Spearman's correlation between metabolite ratios and neuropsychological test scores for PD-MCI.	41
Table 3.6	Spatial distribution of metabolite ratios of patients with PD-CN in different regions.	42
Table 3.7	Spatial distribution of metabolite ratios of patients with PD-MCI in different regions.	42

LIST OF SYMBOLS

ΔE	Energy Difference
ATT_{H_2O}	Attenuation Factors for Water
attmet	Attenuation Factors for Metabolite
B_0	Magnetic Field Strength
Con_{met}	Concentration of Metabolite
f_0	Larmor Frequency
f^{T1}	Spin-Lattice Relaxation Function
f^{T2}	Spin-Spin Relaxation Function
H	Planck Constant
J	Joule
K	Boltzmann's Constant
$N1H_{met}$	Number of Equivalent Protons
$Ratio_{area}$	Ratio of the Resonance Area
T_1	Spin-Lattice Relaxation
T_2	Spin-Spin Relaxation
γ	Gyromagnetic Ratio

LIST OF ABBREVIATIONS

3D	Three-dimensional
ACE-R	Addenbrooke's Cognitive Examination Revised
AD	Alzheimer's Disease
Ala	Alanine
ANOVA	Analysis of Variance
AP	Anterior Posterior
ASL	Arterial Spin Labeling
Asp	Aspartate
CC	Craneocaudal
Cho	Choline
Cr	Creatine
CT	Computed Tomography
DICOM	Digital Imaging and Communications in Medicine
DTI	Diffusion Tensor Imaging
EMCL	Extramyocellular
FID	Free Induction Decay
FOV	Field Of View
FSL	FMRIB Software Library
GABA	γ-Aminobutyric Acid
GDS	Geriatric Depression Scale
Glc	Glucose
Gln	Glutamine
Glu	Glutamate
Gly	Glycine
GSH	Glutathione
IMCL	Intramyocellular
jMRUI	Java-Based Magnetic Resonance User Interface
Lac	Lactate

LCModel	Linear Combination of Model
LR	Left Right
mI	Myo-inositol
MMSE	Mini Mental State Examination
MNI	Montreal Neurological Institute
MR	Magnetic Resonance
MRI	Magnetic Resonance Imaging
NAA	N-Acetyl Aspartate
NAAG	N-Acetylaspartylglutamate
NIfTI	Neuroimaging Informatics Technology Initiative
PCr	Phosphocreatine
PD-CN	Parkinson's Disease with Cognitively Normal
PDD	Parkinson's Disease with Dementia
PD-MCI	Parkinson's Disease with Mild Cognitive Impairment
PET	Positron Emission Tomography
PPM	Parts Per Million
PRESS	Point Resolved Spectroscopy
RF	Radio Frequency
ROI	Region of Interest
rs-fMRI	Resting State Functional Magnetic Resonance Imaging
Sec	Second
STD	Standard Deviation
SDMT	Symbol Digit Modalities
SE	Spin Echo
sI	Scyllo-inositol
SNK	Student-Newman-Keuls
SNR	Signal to Noise
STE	Stimulated Echo
STEAM	Stimulated Echo Acquisition Mode
Tau	Taurine
TE	Echo Time

TM	Mixing Time
TR	Repetition Time
UPDRS	Unified Parkinson Disease Rating Scale
WCST	Wisconsin Card Sorting Test

1. INTRODUCTION

1.1 The Principles of Magnetic Resonance Imaging

Magnetic resonance imaging (MRI) is a non-invasive imaging technique, which can be used in the diagnosis of several diseases including cancer and neurological disorders. In comparison to other imaging modalities, such as computed tomography (CT) and positron emission tomography (PET), MRI is safer, because it does not use harmful ionizing radiation. As a result, even children can be scanned without any harm using MRI.

An MR system includes 6 different components, which are a magnet to produce the main magnetic field, shim coils for creating a homogeneous magnetic field, a radiofrequency (RF) coil to excite and receive an MR signal, a gradient coil for spatial localization, and a computer to process the signal and visualize the final image. In basic MRI physics, once placed into an MR scanner, protons inside the human body align either parallel or anti-parallel to the direction of B_0. Additionally, spins precess about the axis of main magnetic field with a characteristic frequency called the Larmor frequency. Larmor frequency is given by,

$$f_0 = \frac{\gamma B_0}{2\pi}, \tag{1.1}$$

where, B_0 represents a strong external static magnetic field, γ refers to the gyromagnetic ratio for a specific particle like ^{1}H (for ^{1}H,$\gamma/2\pi$=42.576 MHz.T^{-1}).

There is an energy difference between the spin orientations which are parallel or anti-parallel to the external magnetic field. The energy difference can be calculated as,

$$\Delta E = \frac{\gamma h B_0}{2\pi}, \tag{1.2}$$

where, h is the Planck's constant, which is equal to 6.626x10^{-34}J.sec. In thermal equilibrium, the ratio of the number of spins in the upper energy state to the lower state is given by,

$$\frac{N_{up}}{N_{down}} = e^{-\frac{\Delta E}{kT}}, \tag{1.3}$$

where, N_{up} is the number of spins aligned parallel to B_0 (this state is more preferred due to the need for low energy), N_{down} is the number of spins aligned anti-parallel to B_0 (this state is less preferred due to the need for high energy), k is the Boltzmann's constant, which is equal to 1.381 x 10^{-23} J.K^{-1}, and T is the temperature in Kelvin. Equation 1.3 is relevant to low signal-to-noise ratio (SNR) due to the low energy absorption, which results in a grainy image that is not preferred.

An RF pulse is applied perpendicular to the external magnetic field to excite all spins and to select the required frequency range among precessing spins. Once this pulse matches the Larmor frequency, it results in the magnetic moment called, M, to tilt away from the external magnetic field, B_0. When the application of RF pulse is removed, spins want to return the stable state, in which M is parallel to B_0. This return is called 'relaxation' and the signal detected during relaxation is called a 'free induction decay (FID)' signal. FID signal is in the time domain and the Fourier transform (FT) converts it into the frequency domain.

1.1.1 Analysis Tools for Magnetic Resonance Imaging

MR images should be preprocessed before registration. Therefore, brain extraction and image registration could be applied to all MR images. FMRIB Software Library (FSL) [1, 2] (http://fsl.fmrib.ox.ac.uk/fsl/fslwiki/) is a commonly used tool that works on Ubuntu/Linux operating system, which allows for these operations.

1.1.1.1 Brain Extraction (BET)

A head MR image includes skull and brain parts. The skull part is often stripped before image registration. Brain extraction toolbox distributed with FSL is an effective toolbox to get an intensity histogram from the image. Robust upper and lower intensity values can be determined and non-brain tissue (skull, nose vs) can be separated roughly from brain tissue according to histogram thresholds. Head MR images with and without non-brain tissue are shown in Figure 1.1.

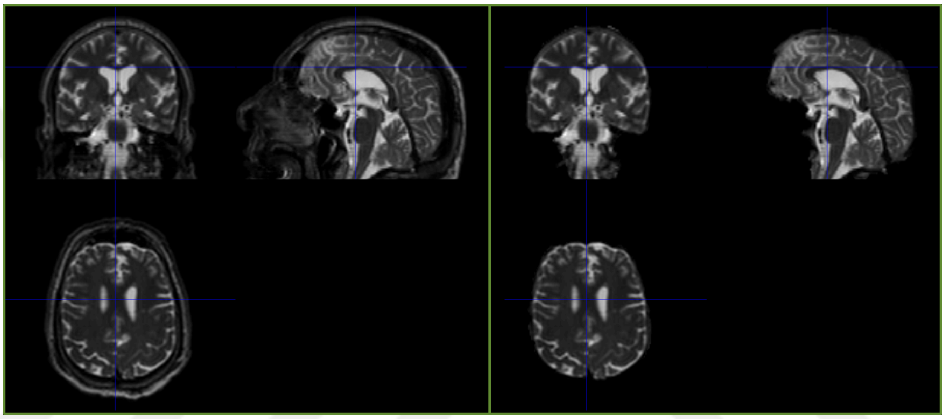

Figure 1.1 A brain extraction example of a T2-weighted MR image.

1.1.1.2 Image Registration

Registration methods are categorized as linear (affine or rigid) and deformable. Compared to affine transformation, rigid transformation seems erroneous and is poor because it does not include aspects like scaling and shearing as well as affine transformation does. Briefly, the reflection, rotation and the translation of the image coordinates are the main component of a rigid transformation. Parametric registration achieves ultimate similarity between the registered and the reference image in order to construct a finite transformation matrix parameter number besides affine and rigid transformations. Rigid transform needs 3 translation and 3 rotation parameters for a 3D image. In addition to these six rotation and translation parameters, affine mapping needs three shear and three scaling parameters. In total, affine transform requires twelve degrees

of freedom parameters. Homogeneous coordinates of reference and moving images can be represented as $[xyz]^{\mathrm{T}}$ and $[x'y'z']^{\mathrm{T}}$ respectively in formula (1.4) that generates a sample mapping [3, 4].

$$\begin{bmatrix} x \\ y \\ z \\ 1 \end{bmatrix} = \begin{bmatrix} a_{11} & a_{12} & a_{13} & tx \\ a_{21} & a_{22} & a_{23} & ty \\ a_{31} & a_{32} & a_{33} & tz \\ 0 & 0 & 0 & 1 \end{bmatrix} \begin{bmatrix} x' \\ y' \\ z' \\ 1 \end{bmatrix}. \tag{1.4}$$

We performed affine linear registration methods by using flirt component of FSL in this study. In the flirt toolbox, affine transformation registers the moving images (input image) to the reference MNI152 brain atlas (template image) and generates an output image. Figure 1.2 shows an example T2-weighted MR image before (left) and after (right) registration to MNI152 brain atlas.

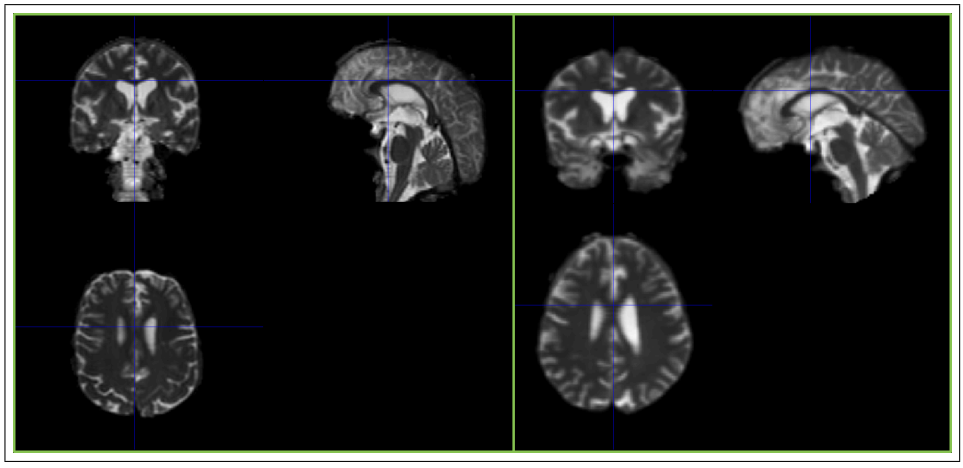

Figure 1.2 An example of T2-weighed image registered to MNI152 brain atlas.

1.2 The Principles of Magnetic Resonance Spectroscopy

The information acquired from MR imaging (MRI) provides a grey-scale anatomical image. In addition to the anatomical image, MR spectroscopy (MRS) provides spectroscopic information about metabolic activity occurring in the region of interest. That means, while MRI uses frequency to encode spatial information, MRS uses it to encode chemical information. This information is represented as an MR spectroscopic signal, called a spectrum. Using FT, FID signal is converted from time domain into frequency domain. The transformation of FID signal into frequency domain enables the visualization of metabolites as distinct peaks. A metabolite is located at a specific location (a fixed frequency value) in the spectrum and the estimation of that location is related to its chemical shift, denoted in parts per million (ppm). Frequency in Hertz (Hz) could be converted into ppm scale as,

$$ppm = \frac{(f_{Hz} \times 10^6)}{f_s} + ppm_{Ref}, \tag{1.5}$$

where, ppm_{ref} is the ppm value of an exact reference resonance, f_{s} is the spectrometer frequency, and f_{Hz} is the resonance frequency of a given metabolite. In ^{1}H MRS, the water resonance is often selected as the reference resonance, which is 4.7 ppm [5]. For example, knowing that the location of creatine peak is -209 Hz below the water's resonance frequency, and if a spectrum is acquired at 3.0 T (127.74 KHz), the chemical shift of creatine at 3T can be calculated as,

$$ppm = \frac{(-209 \times 10^6)}{127.74 \times 103} + 4.7 = 3.07ppm. \tag{1.6}$$

If nuclei are very close to each other, they affect magnetic fields of each other, which results in J-coupling or spin-spin coupling. As a result of J-coupling, the phase of the MR spectroscopic signal vary in time. The unit of J-coupling strength is Hertz (Hz), and it does not vary with the external magnetic field strength.

The appearance of a spectrum can be affected by some parameters that also affect the main contrast in MR imaging. These are diffusion, proton density, T1, T2,

and T2* relaxation. In addition to these, the echo time (TE) is a crucial parameter. TE refers to time between the first pulse application and the initial data acquisition. Repetition time and mixing time are two other parameters that affect the appearance of spectrum like TE. TR refers to time that takes from an excitation pulse application to another pulse application. TM refers to the time delay that occurs in a STEAM sequence between the last two 90° RF pulses. The unit of TE, TR, and TM is milliseconds (ms) [6].

Proton (^{1}H), phosphorus (^{31}P), carbon (^{13}C), nitrogen (^{14}N), sodium (^{23}Na), fluorine (^{19}F) are NMR visible, and proton MRS is the most commonly used MRS technique. There is not any additional hardware necessary for ^{1}H-MRS data acquisition, and most clinical scanners are equipped with ^{1}H-MRS protocols.

1.2.1 Magnetic Resonance Spectroscopic Imaging

MRS is a single voxel spectroscopy, and magnetic resonance spectroscopic imaging (MRSI) creates images from multi voxel spectroscopy. MRSI is also known as chemical shift imaging (CSI). In MRSI, a number of FID signals placed on a 3D-grid forms a metabolic image of the tissue, and instead of single image intensity, each voxel has information regarding several metabolites of the tissue. Low SNR of metabolites restricts the MRSI resolution [7, 8].

This thesis is based on multi voxel ^{1}H-MRSI, and the reason why chemical shift imaging is preferred is to measure the MR signals of a wider selected region of interest instead of a small single region. While single voxel MRS provides the best possible spectrum value from a single limited region, multi voxel MRSI is a superior technique to create metabolic maps of larger areas of the tissue.

1.2.1.1 MR Spectroscopic Imaging Data Acquisition

Point Resolved Spectroscopy (PRESS) and Stimulated Echo Acquisition Mode (STEAM) are the most important and favored ^{1}H MR spectroscopic imaging acquisition sequences. These sequences have common properties both use three slice selective radiofrequency pulses to create free induction decay (FID), stimulated echo (STE), and multiple spin echo (SE) signals [9].

Point Resolved Spectroscopy (PRESS) is a localization method for double spin echo technique and utilizes three slice selective RF pulses with $90° - 180° - 180°$ flip angles in three orthogonal directions. A schematic representation of PRESS pulse sequence for 3D spatial localization can be seen in Figure 1.3.

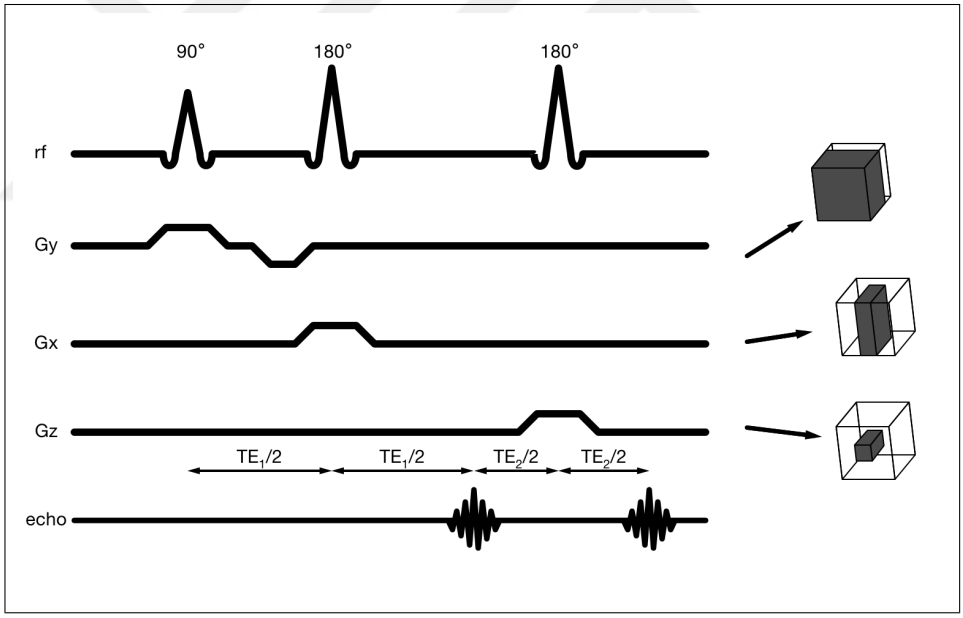

Figure 1.3 PRESS sequence diagram.

The 90° RF pulse and a gradient along x axis are applied and excite the spins to select a slice along y axis. After a time t_1, 180° RF pulse and another gradient along x axis excite the spins to get a column along x and y axes. The first echo is acquired after $2t_1$. The second 180° RF pulse and last gradient along z axis are applied to excite the spins located at a specific value along z axis after a time t_1+t_2. The second echo

occurs after a time t_2 following the second 180° RF pulse. Finally, a spectrum of the selected voxel is formed.

Stimulated Echo Acquisition Mode (STEAM) is a localization method for 3D spatial localization and utilizes three 90° slice selective pulses along x, y, z axes. 90° RF pulses are applied with TE/2 and TM time delays, and the echo is acquired TE/2 after the last RF pulse. G_x, G_y, and G_z gradients are applied along with the three 90° RF pulses. A spectrum is acquired from the intersection of three localizations. A schematic representation of the STEAM pulse sequence for a single voxel spatial location can be seen in Figure 1.4.

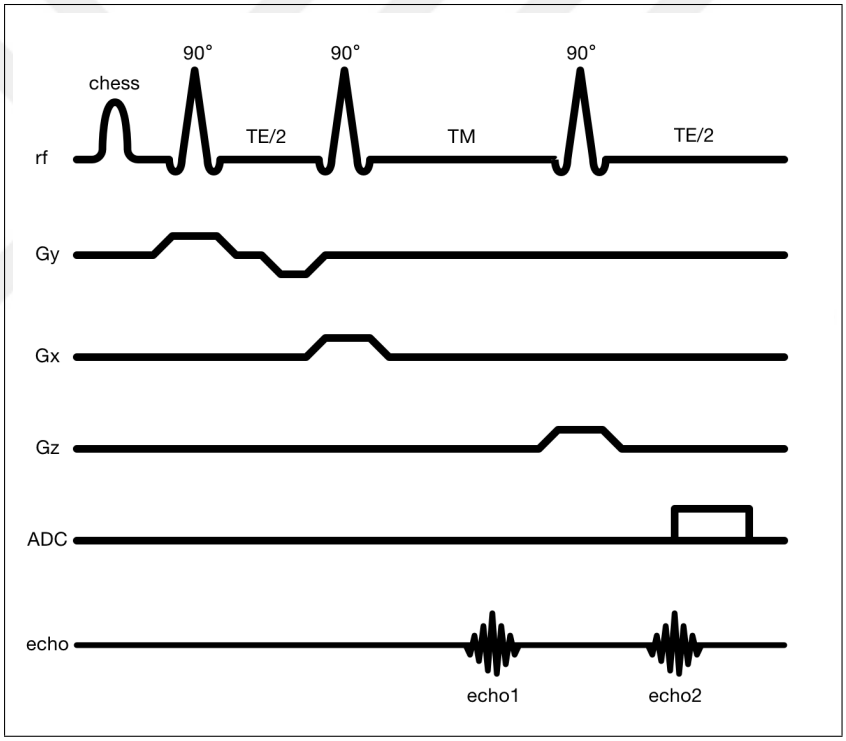

Figure 1.4 STEAM sequence diagram.

PRESS is preferred over STEAM when higher SNR is needed. When short TE is preferred, and the chemical shift artifact is at a minimum, STEAM is used as an alternative to PRESS. STEAM can provide shorter TE at around 20 ms, whereas PRESS can provide TE between 30 ms and 135 ms. In this study, we employed a TE of 52 ms, and preferred PRESS due to its higher SNR.

1.2.1.2 MR Spectroscopic Imaging Data Processing Software

MRS data visualization is possible by using software packages on the scanners. However, researchers need open source, in-house or commercial software packages to process and analyze MRS data. LCModel and jMRUI are two MR spectroscopic data processing software, commonly used in research settings.

LCModel is a commercial software that analyzes in vivo spectrum as a linear combination of model spectra in frequency domain [10]. It is written in C programming language and also it runs only on computers with UNIX or UNIX-like operating systems. Graphical user interface (GUI) of LCModel, abbreviated as LCMGui, calculates the metabolite concentrations such as NAA, Cho, Cr, PCr, mI without any user interaction. It uses Cramer-Rao lower bounds formalism for uncertainties in the concentrations [11]. The formula to calculate the concentration of the metabolites is,

$$Con_{met} = (Ratio_{area}) \times \frac{2}{N1H_{met}} \times \frac{ATT_{H_20}}{att_{met}} \times W_{CONC}, \tag{1.7}$$

where, Con_{met} means concentration of the metabolite, $N1H_{met}$ refers to the number of equivalent protons, ATT_{H_20} and att_{met} indicate the attenuation factors for water and metabolite areas, $Ratio_{area}$ is the ratio of the resonance area of metabolite and unsuppressed water, and W_{CONC} is equal to 35,880 mmol/L that refers to the water concentration in the voxel [12].

jMRUI is a freeware software that analyzes MRS data in time domain [13]. A Java-based GUI is used and works in UNIX, Linux, and Windows environments. Data processing in jMRUI is categorized into two parts: preprocessing and quantitation. Time domain filtering, line shape conversion, and eddy-current correction are applied in the time domain analysis. jMRUI enables to process large data sets and includes a water suppression approach and linear prediction. VARPRO, AMARES, QUEST methods are generally preferred as interactive quantification methods. AMARES is the most popular method that fits Voigt, Lorentzian, and Gaussian peaks to the signal.

The formula to calculate the concentration of the metabolites in jMRUI is,

$$C_M = \frac{S_M}{S_W} \times C_W \times \frac{n_W}{n_M} \times \frac{f_W^{T_1}}{f_M^{T_1}} \times \frac{f_W^{T_2}}{f_M^{T_2}}, \tag{1.8}$$

where, C_W is equal to 35,880 mol/L which indicates the concentration of water in white matter, f^{T1} is spin-lattice relaxation function (1-e$^{\mathrm{TR/T1}}$), f^{T2} is spin-spin relaxation function (e$^{\mathrm{-TR/T2}}$), and n, s, C, M and W refer to the number of chemically equivalent protons, signal intensity, concentration, metabolite, and water, respectively [12].

There has been some studies to compare the quantification results based on LCModel and jMRUI. The main focus on their study was to evaluate the reproducibility of all ^{1}H-MRS metabolites, the reproducibility for GABA and glutamate that is very tricky to determine, lipids in skeletal muscle, the effects of signal to noise ratio and line width on the quantities of human brain spectra. jMRUI was reported to be more sensitive to shape constraints and low SNR than LCModel [14]. In addition to this, jMRUI results were less reproducible than LCModel results, and especially the quantification of small metabolites like glutamate and GABA were less reproducible in jMRUI [15]. The effects of SNR and linewidth on the quantification of human brain spectra were investigated and the results of the study showed that NAA, Cr, and mI to Cr ratios calculated by jMRUI and LCModel were very similar, but LCModel analysis was much better than jMRUI for determining Glx/Cr ratio [16]. Also, the quantification of extramyocellular lipid(EMCL) and intramyocellular lipid (IMCL) concentrations of muscle were similar between these two methods [17]. Additionally, LCModel software doesn't require any user interaction, whereas jMRUI does. So, with its superior quantification capacity and ease of use, LCModel was preferred in this study to quantify metabolites.

1.2.2 Diseases and Diagnosis in ^{1}H-MRSI

The early diagnosis of neuropsychological diseases and cancer plays a crucial role for human health. MRSI, just like computed tomography (CT), gamma camera, pozitron emission tomography (PET), is an important technique in the diagnosis of

several diseases [18, 19]. The change in metabolite concentrations can indicate the type of disease by comparison to the normal values. To obtain the concentrations of MRS signals from a spectrum is the main aim of analysis, and different methods are used for this.

1.2.3 Metabolites in ^{1}H-MRSI

1.2.3.1 Alanine(Ala)

When tumors such as glioma and meningioma are present in the human brain, the level of Ala, which is an amino acid with 0.5 mM concentration in normal tissue, increases. It has two resonances, one of which is a doublet and overlaps with the resonances located at 1.47 ppm, and the other of which is a quartet observed at 3.77 ppm [20].

1.2.3.2 Aspartate (Asp)

Aspartate is an excitatory amino acid that serves as a neurotransmitter. However, it doesn't pass through the blood-brain barrier. Asp is made up of glucose and other precursors. The Asp concentration in the brain is approximately 1-2mM. Its spectrum includes three doublet of doublets. A doublet-of-doublets is located at 3.89 ppm and two other doublets-of-doublets are located at 2.65 ppm and 2.80 ppm [20, 21].

1.2.3.3 γ-Aminobutyric acid (GABA)

It is one of the inhibitory neurotransmitters, whose concentration in human brain is approximately 1 mM. GABA has three resonances, each of which appears at different locations: 1.89 ppm, 2.28 ppm, and 3.01 ppm and overlaps with other more intense resonances. Detection of GABA level can be done feasibly under determined

conditions such as combination of high magnetic fields and spectral fitting [20, 22]. Changes in GABA concentrations may be associated with neuropsychological disorders [23], depression [24, 25], epilepsy [26], and panic disorder [27].

1.2.3.4 Creatine (Cr) and Phosphocreatine (PCr)

Creatine and phosphocreatine levels of ^{1}H-MRSI provide information about the energy metabolism. Cr and PCr are referred to as total creatine (tCr) and has two singlet resonances, the first of which is at 3.03 ppm (Cr) and the second of which is at 3.93 ppm (PCr). The concentrations of Cr and PCr in human brain are between 4.0-5.5 mM and 4.5-6.0 mM, respectively. On the other hand, these concentration values have a small difference in white matter and gray matter. Methyl resonances are the difference between Cr and PCr. Since methyl resonances are too small, a reliable separation of these two metabolites is almost impossible. But methyl resonances can be large enough for a reliable separation of metabolites at a higher magnetic field (7T or higher) [20, 28].

1.2.3.5 Compounds Containing Choline (tCho)

Choline containing compounds are made up of fluid cell membranes and myelin. A singlet located at 3.2 ppm is observed as the mean peak containing choline (Cho), phosphorylcholine (PCh), and glycerophosphorylcholine (GPC), also known as total choline (tCho). Separation of GPC and PCh depends on the methyl protons, which might not be possible because of their close chemical shift. The concentration of the tCho in human brain is about 1-2 mM [29, 30, 31].

Changes in membrane composition are deeply related with changes in tCho [20]. An increased level of Cho peak may demonstrate demyelination, gliosis, ischemia, head trauma, cancer, or Alzheimer's disease. However, a decreased level may be a precursor biomarker for stroke and liver disease.

1.2.3.6 Glucose(Glc)

Glucose is made up of seven protons, out of which five protons belong to hydroxyl groups. Glc has two anomers, which are α and β, respectively. They coexist in aqueous solutions, with an equilibrium concentration of 36% for the former and 64% for the latter. The location of the resonance groups can range between 3.2 ppm and 5.22 ppm. Glc is responsible for storing energy and is a harbinger of a number of compounds. The Glc concentration is approximately 1.0 mM, but sometimes this can change from 1.0 mM to 9.0 mM due to the Glc infusion [20, 32, 33].

1.2.3.7 Glutamate (Glu)

Glutamate is an excitatory neurotransmitter in human brain and a direct precursor and storage for GABA, which is an inhibitory transmitter. Moreover, it takes an important role in the synthesis of small metabolites, proteins, and large peptides. The Glu concentration is about 6-12.5 mM, because its' white and gray matter concentrations could be significantly different from each other Since the resonance groups are located at 2.04 ppm, 2.35 ppm, and 3.74 ppm, they may overlap with resonances of NAA, Gln, and GABA [20]. Glu and Gln levels cannot be indistinguishable at magnetic field strengths of typical clinical MRI scanners, but high magnetic field strengths like 7T can help with resolving these metabolites [34, 35, 36].

1.2.3.8 Glutamine (Gln)

Glutamine is an amino acid, whose resonance groups are located in the range of 2 ppm and 3.8 ppm with a concentration of approximately 2-4 mM. Since Glu and Gln are indistinguishable at low magnetic field strengths, their peaks are often quantified together, and called Glx [37].

1.2.3.9 Glutathione (GSH)

Glutathione has a tripeptide composed of glutamate, glycine, and cysteine, which occurs in reduced (GSH) and oxidized (GSHH) form in living brain. This metabolite, which is an antioxidant, is necessary for maintaining healthy red blood cells because of the demand to keep the ferrous state of hemoglobin. The changes of its levels are important in neurodegenerative disorders, especially in Parkinson's disease [38]. The concentration of this metabolite in human brain is approximately 1-3 mM. GSH is particularly located in astrocytes and resonates as two separate multiplets at 2.15 ppm and 2.55 ppm, three doublet of doublets at 2.93 ppm, 2.98 ppm and 4.56 ppm, and a singlet at 3.77 ppm [39]. Though this metabolite provides critical information, these resonances overlap with NAA, Cr, GABA, Glu, Gln, and Asp. This situation makes the observability of this metabolite not readily available even by using short TE spectra with spectral fitting at very high magnetic field [40].

1.2.3.10 Glycine (Gly)

It is one of the inhibitory neurotransmitters and distributed through the central nervous system. Cr can be converted from Gly. The Gly concentration is approximately 1 mM. A singlet peak that indicates Gly is located at 3.55 ppm. However, it overlaps with mI, which makes it difficult to observe the level of glycine [20].

1.2.3.11 Lactate (Lac)

The production of anaerobic glycolysis finally ends up with lactic acid. Its low concentration and overlap with lipid in normal human brain makes lactate unobservable by using regular in vivo MRS. However, lactate can be observed if its concentration increases due to diseases such as tumors, trauma, stroke, and hyperventilation. Additionally, spectral editing techniques can help in separating lactate and lipid. Lac resonates as a doublet at 1.31 ppm and a quartet at 4.10 ppm [20].

1.2.3.12 Myo-inositol (mI)

It is one of the cyclic sugar alcohols and has four resonance groups, which are a doublet of doublets at 3.52 ppm, a triplet at 3.61 ppm, another smaller triplet at 3.27 ppm, and final triplet at 4.05 ppm. mI has a crucial role for cell growth and it's a storage form for glucose. Readily mI can be detected by combining short TE and high magnetic field strength. mI increases in gliosis and demyelination [20].

1.2.3.13 N-Acetylaspartate & N-Acetylaspartylgluatamate

This amino acid is a marker of the neuronal density, and its reduction indicates neuronal loss such as tumors [41, 42], stroke [43, 44], and multiple sclerosis [45, 46]. Additionally, its' concentration is related to acute metabolic disturbances, such as hypoxia and ischemia. N-Acetyl Aspartate (NAA) has a main singlet resonance at around 2.01 ppm and the main resonance of N-Acetylaspartylgluatamate (NAAG) is located at 2.04 ppm. The concentration of NAA ranges between 7 and 16 mM and NAAG concentration ranges between 0.6 and 3 mM in human brain. The separation of NAAG, which has many peaks overlapping with NAA and glutamate, can only be achieved at high magnetic field strength.

1.2.3.14 Scyllo-inositol (sI or s-Ins)

It is another cyclic sugar alcohols. Also, it is an abundant isomer of inositol following mI. sI level increases in human brain for chronic alcoholism. It contains a singlet located at 3.34 ppm [47, 48].

1.2.3.15 Taurine (Tau)

Taurine is an amino acid, which has a role in modulation and osmoregulation of neurotransmitter action. The concentration of Tau in mammalian brain is approximately 1.5 mM. The spectrum of Tau includes two triplets located at 3.25 ppm and 3.42 ppm, respectively. Tau overlaps with mI and choline, and it is hard to detect it at lower magnetic field strength [49].

1.3 What is Parkinson's Disease?

Parkinson's Disease (PD) was first described in an 1817 paper [50] and it is one of the common neurodegenerative disorders, which has a high incidence rate of over 4 million people aged over 50 within the last two decades. Moreover, this number is projected to double by 2030 [51]. PD incidence is more common with increasing age, like the other neurodegenerative disorders such as Alzheimer's disease.

The characteristic of this disorder depends on aggregation of alpha-synuclein protein in Lewy bodies [52]. It is also associated with reduction of dopamine level due to the dopaminergic cell death and Lewy body aggregations in the substantia nigra [53]. This leads Parkinson's disease and causes loss of control of the voluntary movements. Motor abnormalities are generally seen as rigidity, tremor, postural imbalance, and gait. While motor symptoms is the result of PD influence on movement as a clinical picture, its non-motor symptoms include cognitive and neurobehavioral problems, dysautonomia, and sensory and sleep difficulties [54]. Cognitive dysfunction in PD, which is a non-motor symptom, affecting a person's quality of life, is called Parkinson's Disease Dementia (PDD) [55]. Although the motor changes are more recognizable in the early stages of the disease, cognitive symptoms dominate the later stages with increasing motor symptoms, with a 80% conversion rate to dementia within a few years and aging [56].

Mild cognitive impairment (MCI) has been thought to be a transitional state

of cognitive dysfunction from cognitively normal to dementia [57]. The three subcategories of MCI are single domain amnestic MCI (sd-aMCI), single domain frontal MCI (sd-fMCI), and multiple domains amnestic MCI (md-aMCI). The last subgroup of MCI is one that progresses to clinically overt AD [57, 58, 59]. MCI can be identified based on comprehensive neuropsychological tests. A low score in the Double Memory Test can indicate sd-aMCI that demonstrates impairment in memory function for age and decreased performance. Similarly, a low score in the Trail Making Test B and the Visual Shapes Test can indicate sd-fMCI that demonstrates impaired cognitive memory, which is more common in frontal lobe changes. A low score in Corsi Block-Tapping Test, the Wisconsin Card Sorting Test, and Trail-Making Test A can indicate md-aMCI that demonstrates cognitive impairment in several areas of the brain [60].

1.3.1 Diagnosis of Parkinson's Disease

The Unified Parkinson Disease Rating Scale (UPDRS) is a widely used test for rating the scale of severity for PD and includes 4 different domain assessments, which are mental and mood, daily activities such as how to eat food, dress, and turn in bed, motor manifestations, and complications following treatment. Parts 1, 2, and 4 of the UPDRS test include information given by caregivers or patients. Part 3 of the test examines motor symptoms of participants. As a result, UPDRS is a standardized test in order to examine progression of PD. On the other hand, it cannot assess health-related quality of life (HRQoL) [61].

The Addenbrooke's Cognitive Examination Revised (ACE-R) is a neuropsychological assessment of cognitive functions such as language, memory, visuo-spatial skills, verbal fluency and orientation. ACE-R includes several improvements over the Mini-mental state examination (MMSE), which measures cognitive impairment. MMSE is also known as Folstein test. MMSE is a 30-point questionnaire that measures cognitive impairment. The MMSE comprises simple problems and questions such as the place and time of the test, arithmetic questions such as the series of eight, repeating lists of words, basic motor skills and language comprehension, and this test is commonly

used in medical practice to assess mild cognitive impairment and dementia [61]. A high score close to the total score of ACE-R (100) indicates having better cognitive functions [56]. In our study, whether a patient was PD-MCI or PD-CN was identified according to the ACE-R results. A score of ACE-R bigger than and equal to 83 was identified as PD-CN, and lower than 83 was identified as PD-MCI.

The Stroop test, also called as Stroop effect, is a common neuropsychological test that measures attention and investigates the psychological capacities of a person. This test is based on naming the color of a word, which itself is the name of another color. In the first part of the Stroop test, a word and printed ink of that word are congruent. In the second part of the test, a word and printed ink of that word are not the same. The latter part of this test is harder, compared to the former part, since participants generally read the words without paying attention to the printed ink of the words. When they notice that they said the color of the word wrong, they correct themselves and say the correct color of the word. As a result, the completion of the Stroop test takes a long time [62].

Benton's judgment of line orientation test ensures a versatile measure of spatial perception not only in research but also in clinical setting. This test consists of line segments oriented differently and they should be matched to a response card that shows longer lines. Total score is calculated based on the number of correct items, and adjusted according to age and gender. According to the score of Benton judgment of line orientation test, patients are categorized as normal, mild and severely impaired [63].

The symbol digit modalities test was defined to determine the severity of neurological impairment of patients. The impairment of neurocognitive functions such as motor, speed, attention, and visual scanning could be investigated with the SDMT. A series of symbols are matched to a sample set of symbols that are numbered, and then participants are asked to match the symbols with the sample set, and write down the corresponding numbers within 90 seconds. The test is conducted not only in written but also in oral form [64].

Wisconsin card sorting test, abbreviated as WCST, is a neuropsychological test that measures thinking, cognitive flexibility, and impairment. There are two decks of cards and cards have different colors, shapes, and number of shapes. The first deck of cards is used as stimulus card that is expected to match the second deck of cards. The second deck of cards is shown to a participant one by one. As a result, the participant is expected to match the first deck of cards with the second one according to the rules which is not told to him/her. The participant should match the cards by defining his rules based on the feedback given after each correct answer [65].

1.4 Assessment of MRS Findings in PD-CI, PD-MCI, and PDD

Current standards for diagnosis and assessment of the progression of Parkinson's disease are clinical and neuropsychological measures. Therefore, Parkinson's disease has been one of the remarkable academic research subjects and PD-CI, PD-MCI, and PDD groups has been compared to each other to find the relationship of the progression of the disease due to the fact that 60% of patients with PD-MCI may be at the risk of developing dementia [66, 67, 68].

A number of studies has been done to observe biomarker differences among people with PD-CI, PD-MCI, PDD and healthy. A study was completed with 14 participants with PDD, 12 people with PD and 13 people as a control subjects in 2002 and showed that PDD group had low NAA levels in the occipital region compared to PD and control groups. They advocated that this metabolite values were associated with neuropsychological performance except severity motor impairment and a low NAA level in the occipital lobe could be a biomarker for PDD [69]. Another study was done with 12 people with non-demented mild to moderately affected PD and 10 controls. It reported that patients with PD had reduced NAA/Cr ratios in the posterior cingulate gyrus (PCG), which was contradict the report that a lower NAA/Cr in PCG could be a specific biomarker of AD [70, 71]. Performance on a memory task would correlate with NAA/Cr [71]. Two studies of Griffith and friends concluded that the NAA/Cr ratios of ^{1}H-MRS of patients with PDD decreased compared to healthy controls and

non-demented PD in PCG besides lower Glu/Cr ratios [72, 73]. A study completed with three groups which were 66 patients with PD-MCI, 70 patients with PD-CN, and 74 healthy controls indicated that ^{1}H MRS of occipital lobe in PD-MCI patients, has revealed a reduced NAA/Cr ratios compared to healthy controls. On the other hand, ^{1}H MRS of posterior cingulate in PD-MCI has revealed the increased Cho/Cr ratios. Furthermore, there was not found any significant metabolite differences in basal ganglia and substantia nigra [74]. Almuqbel, M. and friends [75] reported that PDD had a lower NAA/Cr ratio and a higher Cho/Cr ratio in the posterior cingulate cortex compared to healthy controls at the baseline. However, there was not any relationship found between MRS metabolite ratios and change in cognitive status at over time. A new strategy was used to help to ROI placement for unbiased anatomical position by means of atlas-based automated protocol during the MR and MRS scan as a different MRS study [76].

As can be seen, previous studies related to PD-CI, PD-MCI, and PDD using ^{1}H-MRS provided important information as predictive neurobiomarkers in the different brain regions affected such as occipital lobe, posterior cingulate gyrus, basal ganglia, and substantia nigra. These studies were performed with single voxel ^{1}H-MRS and mainly investigated metabolites were NAA, Cho, Cr, mI, and Glu.

1.5 The Objective of the Study

Previous studies related with spectroscopy of PD-MCI acquired single voxel ^{1}H-MRS data in only a few areas of the brain, and did not study several regions at the same time using multi-voxel MRSI. Additionally, they did not register the MRS data to a brain atlas or created an automated MRSI data analysis tool to evaluate MRSI data along with other MR modalities in a group analysis to define a biomarker. Therefore, there is a need for an automated and atlas registered ^{1}H-MRSI data analysis approach that would enable a faster and more accurate data analysis.

The goal of this study is to find novel ^{1}H MR spectroscopic based biomarkers

of PD-MCI by comparison with ^{1}H-MRSI data of PD-CI patients. For this purpose, we developed an MRSI data analysis tool that would create ^{1}H MR spectroscopic peak parameter maps out of raw MRSI data, overlay them onto reference T2-weighted MR images, and afterwards register overlaid metabolite maps to an MNI152 brain atlas.

2. MATERIALS and METHODS

2.1 Subjects

A total of 40 patients with PD were included in this study, and 19 of these patients were PD-MCI, and the rest were PD-CN. Istanbul University Clinical Research Ethics Committee approved the study protocols concerning human welfare, and all participants in this study provided written informed consent. Patients showing any signs of depression, using anti-depression drugs, or that have less than 5 years of education were excluded from this study for a more homogeneous data distribution. The participants were matched according to their age, gender, and education background. The patients had ages between 40 and 80, and education level range was 5-15 years. Table 2.1 provides some information about the subject demographics included in this study.

Table 2.1
The demographic information of the subjects included in this study.

Patient #	Status of PD	Age	Gender	Education Level	Patient #	Status of PD	Age	Gender	Education Level
1	PD-MCI	57	M	8	21	PD-CN	68	M	10
2	PD-MCI	66	M	15	22	PD-CN	78	M	11
3	PD-MCI	60	M	7	23	PD-CN	54	M	15
4	PD-MCI	68	M	5	24	PD-CN	68	M	15
5	PD-MCI	64	M	5	25	PD-CN	47	M	15
6	PD-MCI	46	M	5	26	PD-CN	46	M	12
7	PD-MCI	58	M	11	27	PD-CN	52	M	12
8	PD-MCI	60	M	11	28	PD-CN	42	M	11
9	PD-MCI	42	F	5	29	PD-CN	70	F	8
10	PD-MCI	55	M	11	30	PD-CN	54	F	11
11	PD-MCI	55	M	5	31	PD-CN	52	F	11
12	PD-MCI	70	F	5	32	PD-CN	81	F	8
13	PD-MCI	74	M	5	33	PD-CN	56	M	5
14	PD-MCI	61	F	11	34	PD-CN	53	F	15
15	PD-MCI	56	F	11	35	PD-CN	65	M	7
16	PD-MCI	54	F	5	36	PD-CN	58	M	5
17	PD-MCI	76	M	11	37	PD-CN	58	F	5
18	PD-MCI	57	F	5	38	PD-CN	43	M	7
19	PD-MCI	62	M	5	39	PD-CN	75	M	15
20	PD-CN	60	M	5	40	PD-CN	50	M	5

2.2 Diagnostic Assessment

All participants got examined in order to assess their motor system status. Neuropsychological and clinical examinations based on UPDRS, MMSE, ACE-R, STROOP, line orientation, SDMT, Wisconsin, and GDS were applied. Each subject was classified as PD-CN or PD-MCI by experienced neurologists according to the clinical examination results and neuropsychological test scores.

2.3 Data Acquisition MR Protocol

After motor and cognitive assessments, ^{1}H-MRSI data and T2-weighted anatomical MR data were acquired with a clinical 3T MR scanner (Philips Medical Systems, Best, Holland) at Hulusi Behcet Life Sciences Research Center, Istanbul University. Patients were positioned in MR scanner with a 32-channel 1H head coil. T2-weighed MRI and ^{1}H MRSI data were acquired and their protocol parameters are given in Table 2.2. ^{1}H-MRSI data was acquired from the supratentorial brain. The ^{1}H-MRSI protocol that was employed in this study had a restriction on the number of slices that can be acquired at once. So, two consecutive ^{1}H-MRSI data acquisitions were performed from two regions of the brain, each comprising of 3 slices. Figure 2.1 shows the two different brain regions of ^{1}H-MRSI data acquisition in a selected patient. ^{1}H-MRSI data of the occipital lobe, posterior cingulate, basal ganglia, right and left temporoparietal cortex, substantia nigra, the lentiform nigra, and striatum were assessed. Additionally, T1-weighted MRI, resting state functional magnetic resonance imaging (rs-fMRI), diffusion tensor imaging (DTI), and arterial spin labelling (ASL) MRI data were acquired in each patient.

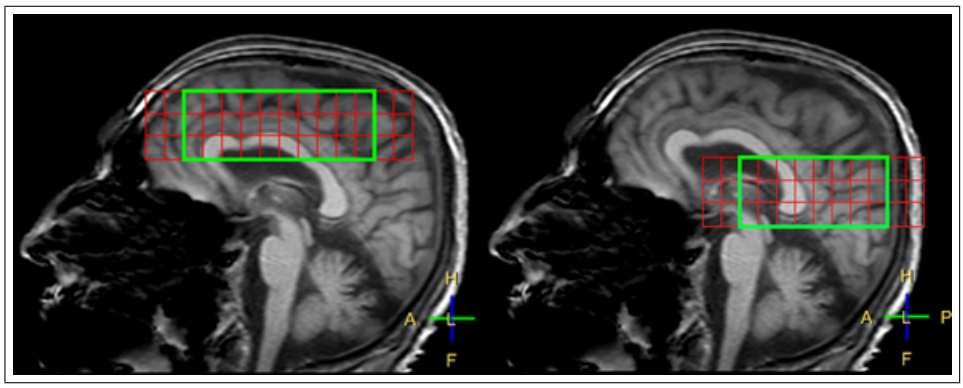

Figure 2.1 The sagittal view of two different regions of interest in an example patient.

Table 2.2
MR Acquisition parameters for T2-weighted MR image and ^{1}H-MRSI.

T2-weighted MRI Parameters	**^{1}H-MRSI Parameters**
TR=10243 ms	TR=1000 ms
TE=80 ms	TE=52 ms
1 time point	1024 time points
Flip angle=90°	Flip angle=90°, 180°, and 180°
Acquisition matrix=128x128x90	Acquisition matrix=14x14x3
FOV=240 mm	FOV=140 mm
Slice thickness=2 mm	Slice thickness=36 mm
Scan time=3.5 min	Scan time=8 min
	Voxel size=10x10x10 mm

2.4 Post Processing

Raw ^{1}H-MRSI data was exported and analyzed outside of the scanner. The raw data included an .spar file that had acquisition parameter information, and an .sdat spectroscopic data file. LCModel was used to automatically fit spectra in each voxel, to obtain the concentration values of all metabolites, the standard deviation (%std) of the quantification, and the ratios of metabolite concentrations to Cr+PCr. The LCModel graphic output provided the estimated spectrum, a calculated residual noise spectrum, and a baseline spectra for fitting as can be seen in Figure 2.2.

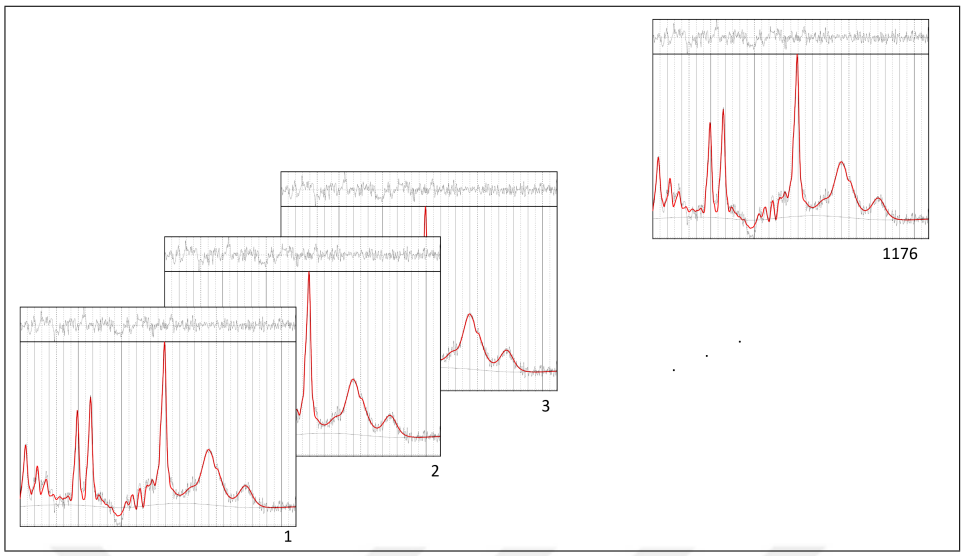

Figure 2.2 Example LCModel outputs.

1176 MRS voxels were acquired for each patient, and were analyzed one by one in LCModel. Considering the total number of voxels, analyzing more than 1000 MRSI data with many metabolites one by one was impossible for us because of the challenge to determine each voxel localization and it would be very time consuming to assess all LCModel outputs. ^{1}H MR spectroscopic peak parameter maps of each slice were created out of LCModel outputs by using an in-house software written in MATLAB (The Mathworks Inc., Natick, MA). First, LCModel outputs were parsed by using a text reader. Then, each voxel result was positioned into a 3D grid in accordance with the Philips MRSI data format shown in Figure 2.3. For each metabolite map, the voxels were assigned the value of the ratio of that metabolites to Cr+PCr in the corresponding location. In this study, NAA+NAAG, GPC+PCh, Glu+Gln, mI and the ratios of the level of these four metabolites to the level of Cr+PCr metabolite maps were produced. Figure 2.4 shows three different NAA+NAAG metabolite maps that belongs to 3 slices acquired from the top portion of the brain of a subject.

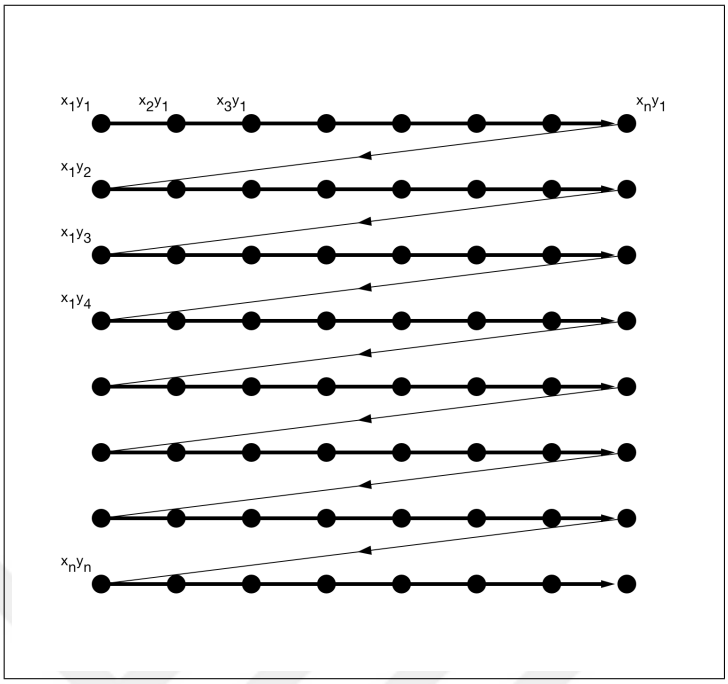

Figure 2.3 Image space for Philips MRSI data.

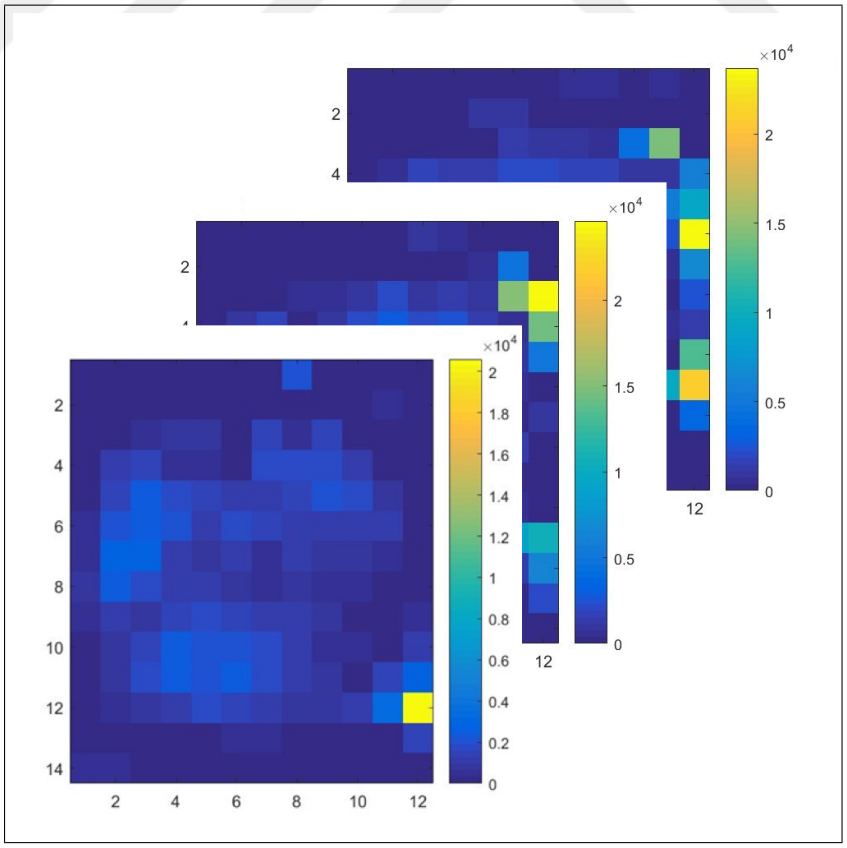

Figure 2.4 NAA+NAAG/Cr+PCr peak parameter maps that belongs to 3 slices.

For determining metabolic profiles of several parts of the brain, we first visually assessed the location of the particular area of interest. As an example, the circle marked in yellow in Figure 2.5 indicates the area of anterior cingulate in a sagittal T2-weighted structural image.

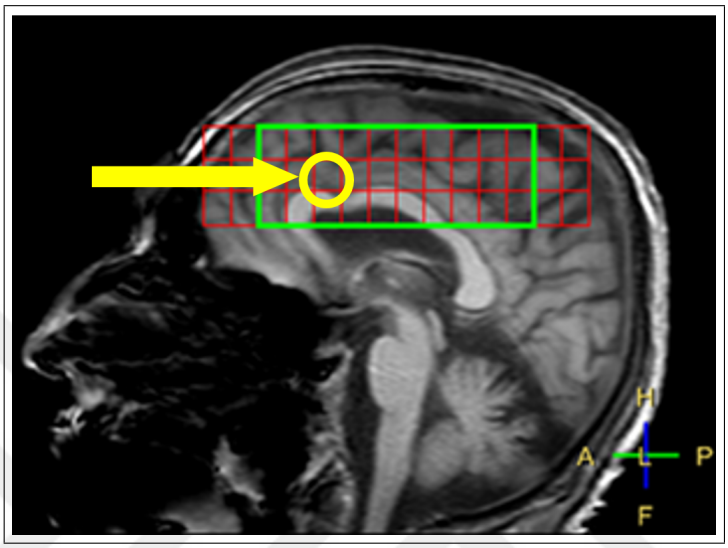

Figure 2.5 Voxel marked in yellow circle shows anterior cingulate.

Then, MNI 152 brain atlas was used to determine the region marked in yellow in the axial ^{1}H MR spectra. The region of anterior cingulate was next to the centerline in axial view of the MNI152 atlas (Figure 2.6).

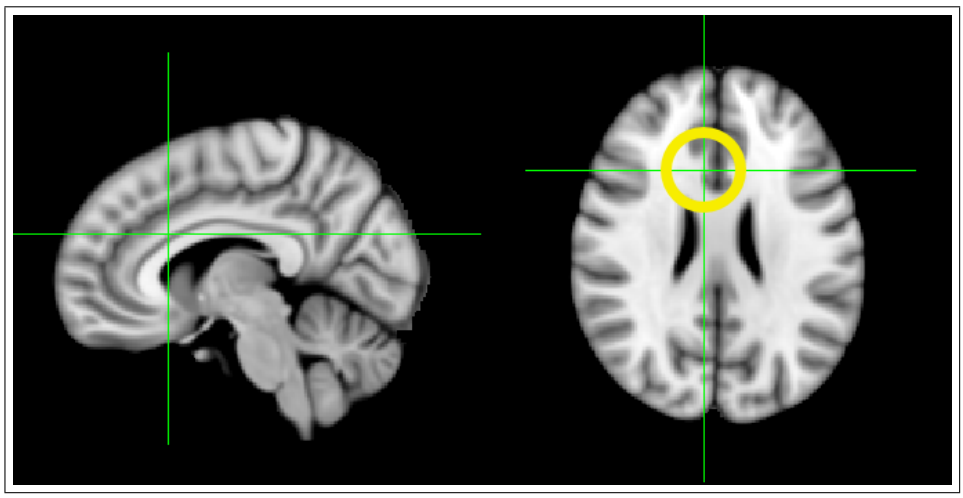

Figure 2.6 Sagittal and axial MNI152 brain atlas with the corresponding voxel marked in yellow.

Considering the anatomical location of the cingulate gyrus, a voxel of the second slice of ^{1}H-MRSI that matched to the location at the MNI152 brain atlas was selected in the axial metabolite map, which refers to the yellow circle in Figure 2.7.

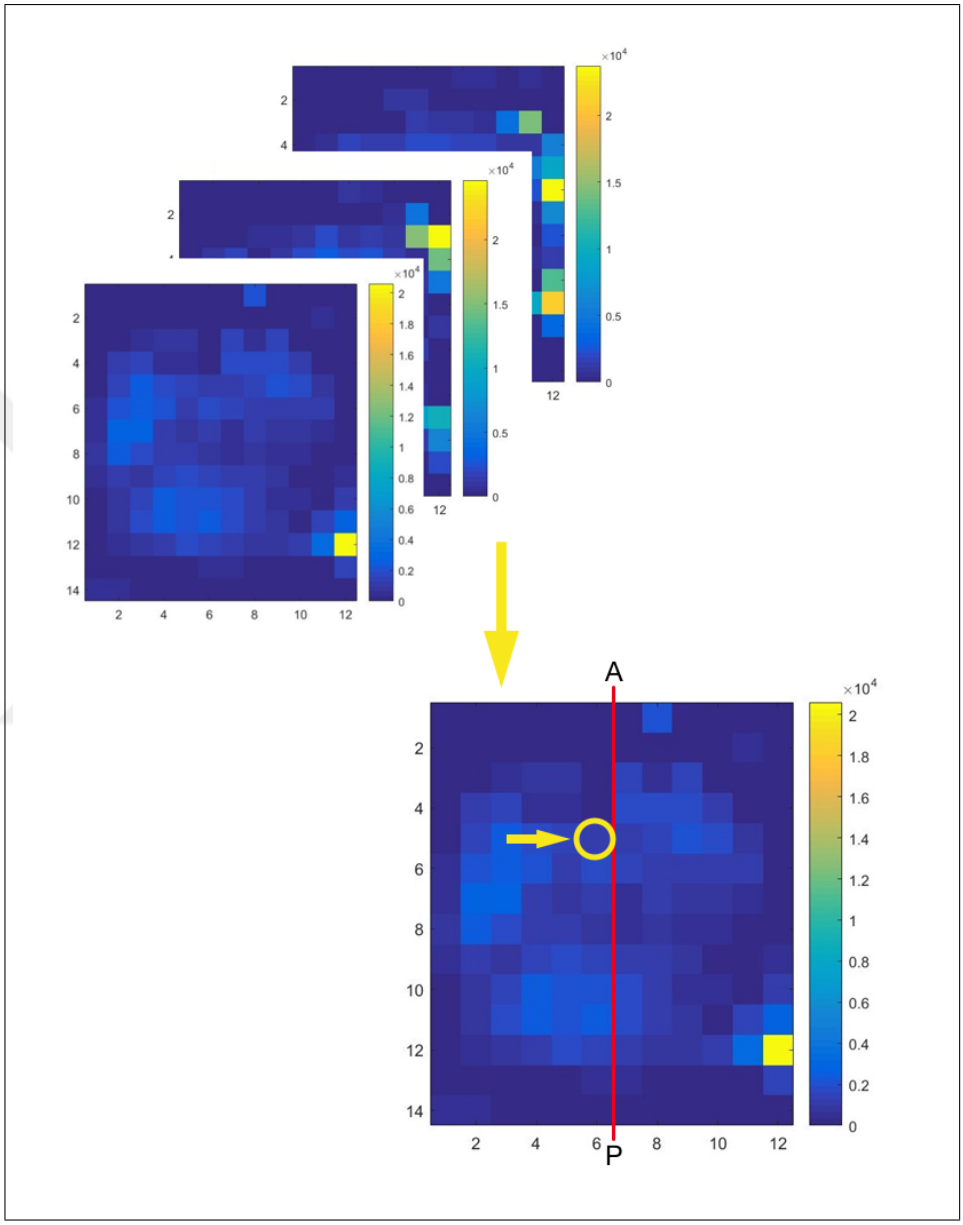

Figure 2.7 Example selection of a voxel in a metabolite map.

Determining all region including cingulate gyrus, frontal lobe, thalamus, and occipital lobe was difficult in the ^{1}H MR spectroscopic peak parameter maps due to the different platforms including anatomical T2-weighted MR images, metabolite maps, and MNI 152 brain atlas. We developed a novel program in MATLAB to minimize

the hassle in voxel selections. ^{1}H MR spectroscopic peak parameter maps were first overlaid onto reference T2-weighted images considering the anterior posterior (ap)/left right (lr)/ craneocaudal (cc) ROI off center, size, and angulation. ^{1}H MR spectroscopic peak parameter maps overlaid onto reference T2-weighted images had 3 dimensions, one of which referred to slice number and a particular range of these slice numbers provided the information of ^{1}H MRSI acquired from that region.

The image seen in Figure 2.8 can be used to find the voxels related to region of interest (ROI) but it has still difficulty to delineate the exact anatomical region and to compare the data in the group analysis.

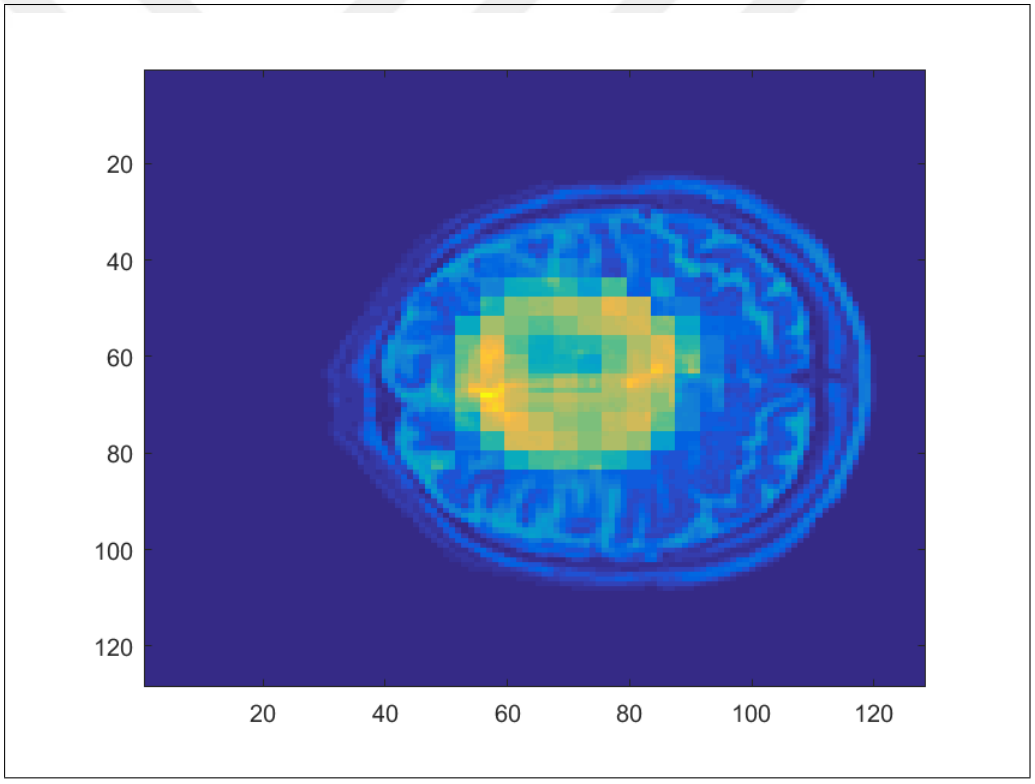

Figure 2.8 Metabolite map overlaid onto reference T2-weighted image.

Therefore, a software package was developed in MATLAB to make the whole process automatically run by pushing a button. Figure 2.9 shows that graphical user interface (GUI) of the software package that requires 4 inputs. These are spar file to read ap, lr, cc size, and three different axis angulations, LCModel results for the ratios

of different metabolites, T2-weighted MRI DICOM image for image information that will be used to for overlay, and T2-weighted MRI brain after BET extraction to overlay the metabolite maps onto it. In this thesis, all metabolite ratio results were processed, and were used to create metabolite maps overlaid onto reference T2-weighted image in this easy to use software package. The resultant overlaid metabolite maps were in NIFTI format, and they had the same image information of the original T2-weighted MR images. The signal intensity in each location of the overlaid map indicated the ratio of a given metabolite to Cr+PCr.

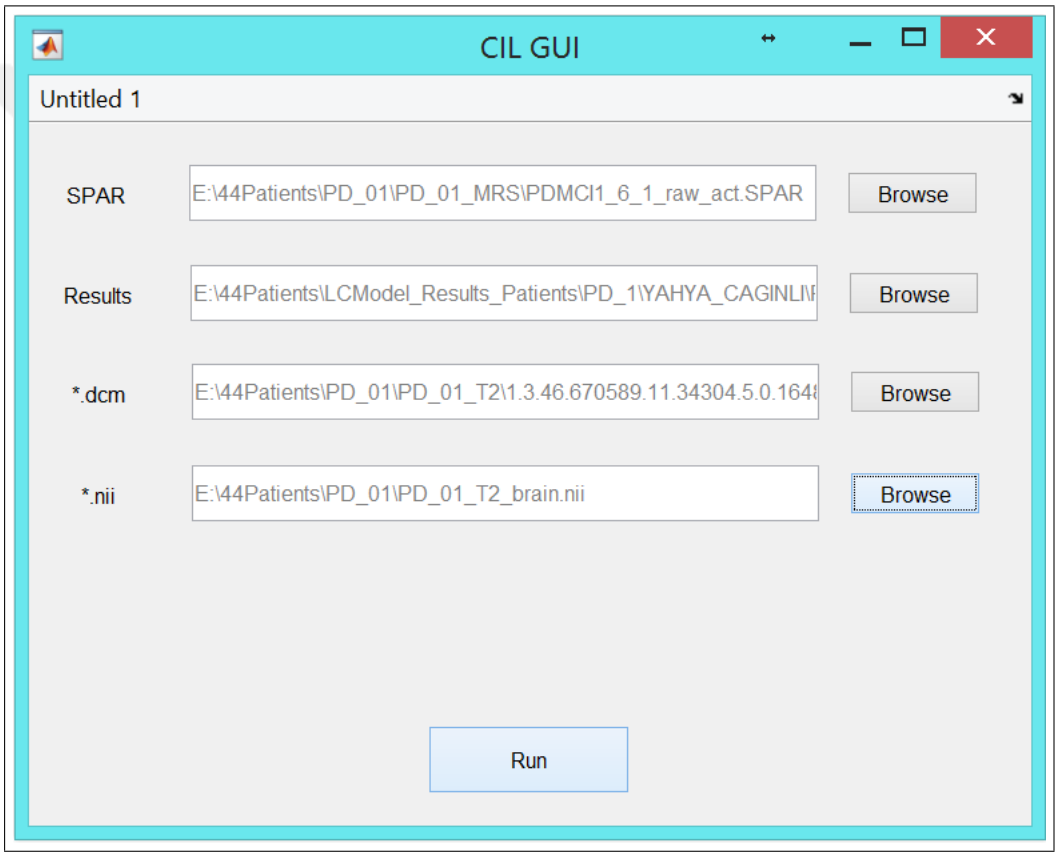

Figure 2.9 The GUI of the data analysis tool.

2.4.1 Registration of Metabolite Maps Overlaid onto Reference T2-weighted MR Image to MNI 152 Atlas

Registration of metabolite maps overlaid onto reference T2-weighted MR image to MNI 152 atlas consisted of two steps. First, original T2-weighted MR images were

registered onto the MNI 152 brain template, and a registration matrix was obtained (Figure 2.10).

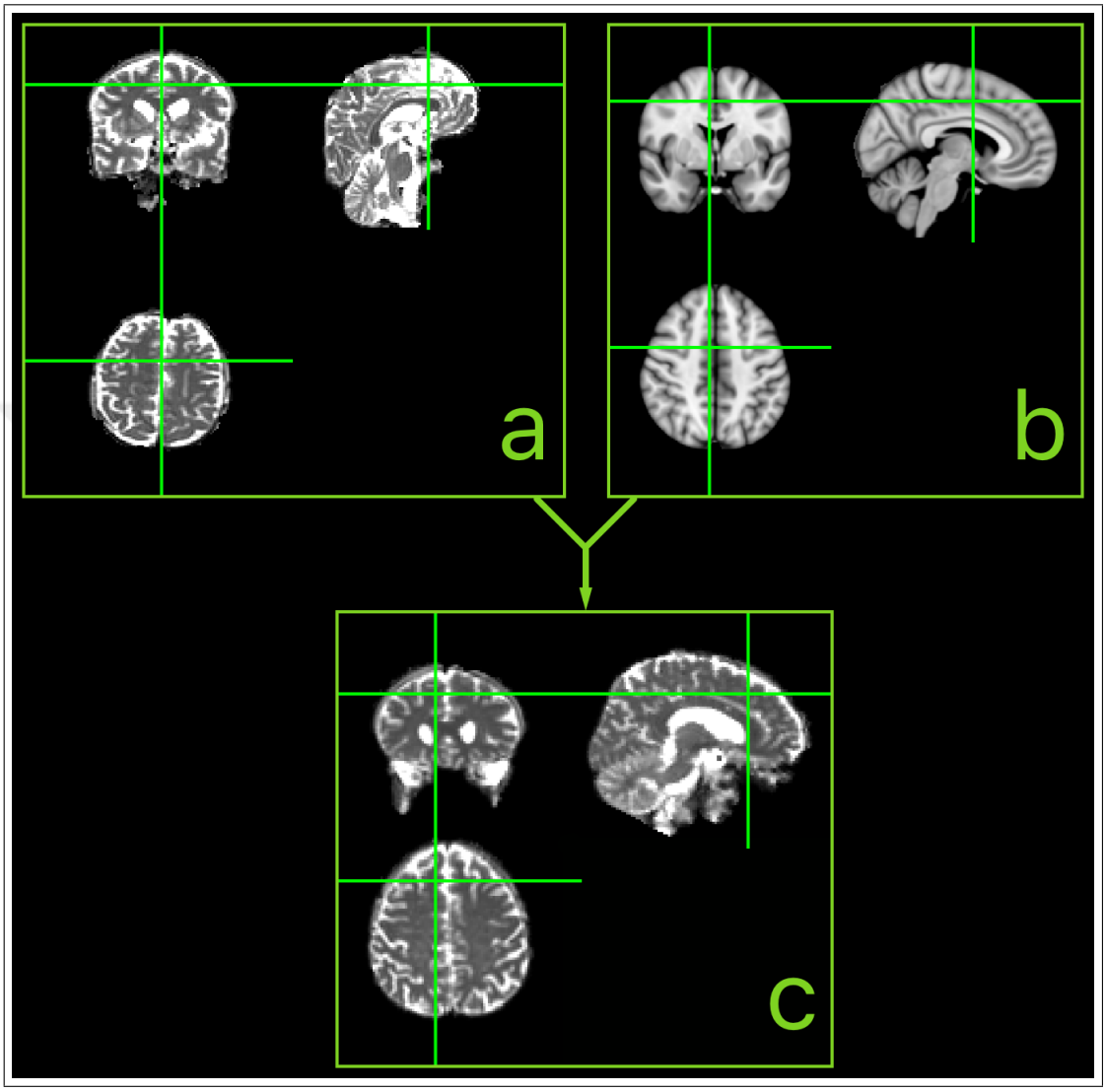

Figure 2.10 a. raw T2-weighted image b. MNI 152 brain atlas c. registered T2-weighted image to MNI 152 brain atlas (coronal, sagittal, and axial).

The second part consisted of registering a metabolite map overlaid onto the brain extracted T2-weighted MRI to MNI 152 brain atlas by applying the same registration matrix acquired from the first part (Figure 2.11). FSL program was used to register original T2-weighted MR images to MNI atlas and to apply the same registration matrix to different ^{1}H-MRS metabolites maps.

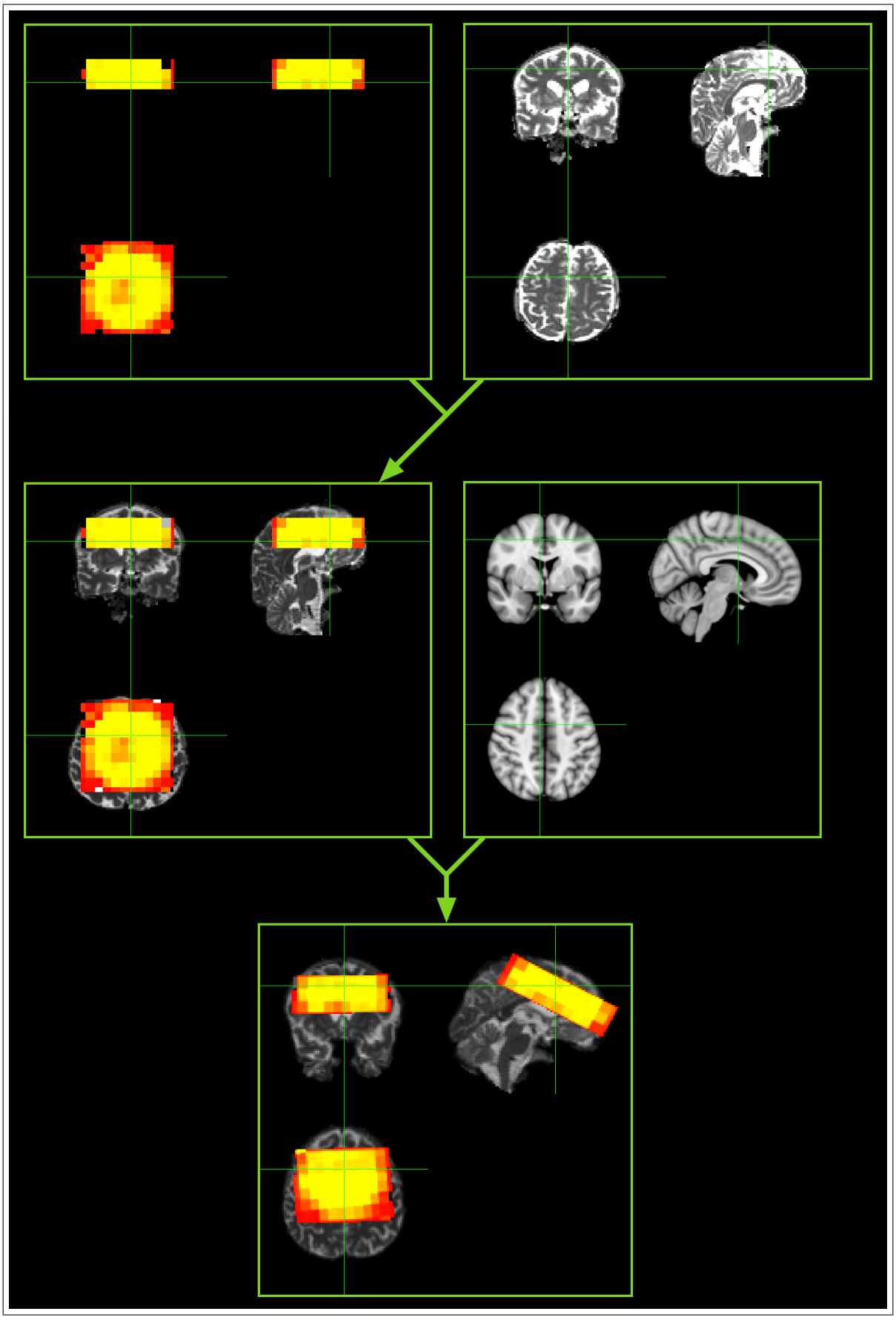

Figure 2.11 MRSI registration steps.

2.5 Region of Interest Analysis

After registration, FSL atlas toolbox was used to define ROIs of several brain regions and to get the signal intensity of that region. MNI 152 standard space T1 weighted average structural template image, Harvard-Oxford cortical and subcortical structural atlases, Talairach atlas, MNI structural atlas, Oxford thalamic connectivity atlas were available in the FSL atlas toolbox. MNI 152 and Harvard-Oxford cortical and subcortical structural atlases were used to define ROIs for precuneus, occipital lobe, posterior cingulate gyrus, white matter, thalamus, frontal lobe and cerebral gray matter.

2.6 Statistical Analysis

Mann-Whitney ranksum test with Bonferroni multiple comparison correction was used to understand the differences of metabolite ratios and neuropsychological test scores between PD-MCI and PD-CN. Spearman rank correlation coefficient test was used to assess if there was any correlations between neuropsychological test scores and metabolite ratios. Friedman's statistic test was used to assess the difference of metabolite ratios in all brain regions of PD-MCI or PD-CN patients. Student-Newman-Keuls (SNK), which is a post hoc test algorithm, was applied to observe which pairwise regions statistically significantly differed for PD-MCI and PD-CN patients. IBM SPSS program was used in all statistical analysis.

3. RESULTS

3.1 Demographics and Neuropsychological Assessments

Of the 40 patients included, 12 were women and 28 were men. The ratio of female to male patients was 13/6 in PD-MCI and 15/6 in PD-CN. The mean age of PD-MCI patients was 60.05±8.55, and PD-CN patients was 58.57±11.29. The mean education level was 7.68±3.26 years in PD-MCI and 9.90±3.79 years in PD-CN. The number of female participants with PD-CN was lower than female participants with PD-MCI. There was a small difference in education level of PD-MCI and PD-CN patients. Table 3.1 shows the ACE-R, GDS, UPDRS, STROOP, line orientation, and SDMT scores of all patients.

Table 3.2 shows the mean results of neuropsychological tests and differences between these scores in PD-MCI and PD-CN. According to the results, there was a statistically significant difference between the ACE-R scores of patients with PD-MCI and PD-CN. Patients with PD-CN had higher ACE-R scores than patients with PD-MCI. The GDS, UPDRS, STROOP, line orientation, and SDMT scores were not statistically significantly different between PD-MCI and PD-CN.

3.2 MRSI Markers

Glu+Gln, Cho, mI, and NAA+NAAG to Cr+PCr metabolite ratios in seven different brain regions, which were precuneus, occipital lobe, posterior cingulate gyrus, cerebral white matter, thalamus, frontal lobe, and cerebral gray matter were analyzed in this study. The average metabolite ratios and the comparison results of PD-MCI and PD-CN are listed in Table 3.3.

Table 3.1
Neuropsychological test scores of all patients.

#	STATUS	ACE_R	GDS	UPDRS	STROOP(sec)	LINE	SDMT	#	STATUS	ACE-R	GDS)	UPDRS	STROOP(sec)	LINE	SDMT
1	PD_CN	84	9	60	64	12	16.36	21	PD_CN	85	11	87	49	22	20.9
2	PD_MCI	76	7	46	57	16	18.18	22	PD_CN	85	9	25	81	24	28.18
3	PD_MCI	82	1	22	47	25	32.72	23	PD_CN	91	2	45	60	14	31.81
4	PD_CN	89	11	57	69	24	17.27	24	PD_MCI	72	7	55	86	19	15.45
5	PD_CN	84	5	32	97	27	24.54	25	PD_MCI	69	2	30	12	18	16.36
6	PD_CN	90	5	70	65	26	23.63	26	PD_MCI	76	4	34	77	14	18.18
7	PD_CN	90	10	45	47	26	21.81	27	PD_MCI	82	7	65	93	20	29.09
8	PD_CN	98	11	53	27	27	48.18	28	PD_CN	92	0	45	28	28	35.45
9	PD_MCI	72	13	56	46	26	30.9	29	PD_CN	89	4	36	39	22	26.36
10	PD_CN	89	10	54	40	25	30.9	30	PD_MCI	72	3	51	23	21	24.54
11	PD_MCI	72	10	79	60	21	18.18	31	PD_MCI	75	3	17	26	24	34.54
12	PD_CN	84	8	47	39	24	36.36	32	PD_CN	88	8	38	46	22	18.18
13	PD_MCI	71	9	74	72	18	12.72	33	PD_CN	95	11	30	37	18	26.36
14	PD_CN	92	3	40	89	29	31.81	34	PD_MCI	68	2	49	55	24	19.09
15	PD_CN	84	11	46	79	23	27.27	35	PD_CN	85	4	70	48	26	23.63
16	PD_MCI	68	2	13	14	22	18.18	36	PD_CN	86	5	56	64	20	22.72
17	PD_MCI	80	9	70	54	26	34.54	37	PD_MCI	80	4	66	33	13	20
18	PD_MCI	82	11	33	23	25	31.81	38	PD_MCI	66	11	66	55	27	14.54
19	PD_CN	80	10	46	29	18	31.81	39	PD_CN	87	2	80	48	25	23.63
20	PD_MCI	79	7	27	68	25	28.18	40	PD_MCI	72	10	43	67	19	18.18

Table 3.2
Comparisons of the neuropsychological test scores.

	Mean± std (PD-MCI)	Mean± std (PD-CN)	P
ACE-R	74.42±5.18	87.95±4.24	<0.0001*
GDS	6.42±3.71	7.09±3.61	0.43
UPDRS	47.15±20.06	50.57±16.08	0.67
STROOP	50.94±23.87	54.52±20.22	0.68
Line Orientation	21.21±4.19	22.95±4.44	0.16
SDMT	22.91±7.40	27.01±7.42	0.11

The p-values were calculated by using a Mann-Whitney rank-sum test with Bonferroni correction (*p<0.008)

After multiple comparison correction, there was a trend for a higher mI/Cr+PCr in cerebral white matter in PD-MCI patients than PD-CN (1.35±1.25 vs 0.79±0.40, p=0.02). In addition, there was a trend of a higher Cho/Cr+PCr in frontal lobe in PD-MCI than PD-CN (0.35±0.07 vs 0.3±0.04, p=0.04). There was not any other significant metabolic differences in other regions between PD-MCI and PD-CN groups.

3.3 Pairwise Correlation

Table 3.4 shows the mean (±std) metabolite intensity ratios in each region in PD-CN and their correlations to the neuropsychological test scores. Spearman's rank correlation coefficient (r), and p-values are reported. According to the results, there was negative correlation between GDS scores and NAA+NAAG/Cr+PCr in thalamus (r= 0.434, p=0.049). The test score of line orientation had a negative correlation with Cho/Cr+PCr (r=0.452, p=0.040) and mI/Cr+PCr (r=0.656, p=0.001) in posterior cingulate gyrus. There was also positive corellation between SDMT scores and Cho/Cr+PCr in posterior cingulate gyrus (r=0.486 , p=0.025). There weren't any significant correlations between ACE-R, UPDRS, and STROOP test scores and the metabolite ratios in these selected seven regions.

Table 3.3
Comparisons of different metabolite ratios in different brain regions.

PD-MCI vs. PD-CN		Glu+Gln/(Cr+PCr)	Cho/(Cr+PCr)	mI/(Cr+PCr)	NAA+NAAG/(Cr+PCr)
Precuneus	PD-MCI	2.49±1.83	0.28±0.06	1.52±0.81	1.43±0.32
	PD-CN	2.42±2.09	0.27±0.06	1.18±0.64	1.53±0.25
	p	0.7	0.43	0.1	0.28
Occipital Lobe	PD-MCI	1.66±0.67	0.26±0.06	2.39±4.16	1.66±0.54
	PD-CN	1.42±0.34	0.26±0.06	1.24±0.97	1.5±0.22
	p	0.32	1	0.18	0.05
Posterior Cingulate Gyrus	PD-MCI	2.24±1.23	0.28±0.04	0.96±0.55	1.26±0.17
	PD-CN	1.92±0.93	0.27±0.04	0.73±0.24	1.26±0.13
	p	0.53	0.37	0.59	0.77
Cerebral White Matter	PD-MCI	2.16±1.75	0.64±1.31	1.35±1.25	1.77±1.29
	PD-CN	1.71±0.93	0.33±0.05	0.79±0.40	1.37±0.19
	p	0.09	0.46	0.02*	0.2
Thalamus	PD-MCI	3.04±3.07	0.38±0.11	1.44±0.85	1.77±0.61
	PD-CN	2.28±1.85	0.45±0.24	1.25±0.81	1.77±0.68
	p	0.65	0.37	0.48	0.96
Frontal Lobe	PD-MCI	3.63±5.71	0.35±0.07	1.29±0.60	1.34±0.41
	PD-CN	2.62±2.33	0.3±0.04	1.14±0.70	1.38±0.30
	p	0.51	0.04*	0.41	0.82
Cerebral Gray Matter	PD-MCI	3.34±7.13	0.32±0.06	1.78±2.61	1.18±0.24
	PD-CN	2.54±2.00	0.32±0.08	1.06±0.59	1.49±0.64
	p	0.21	0.86	0.27	0.05

Mann-Whitney rank-sum test: *p<0.05, with Bonferroni correction: **p<0.001.

Table 3.5 shows the mean (±std) metabolite intensity ratios in each region and their correlations to the neuropsychological test scores in PD-MCI. There was a positive correlation between ACE-R scores and NAA+NAAG/Cr+PCr in the posterior cingulate gyrus (r=0.532, p=0.019). There was a negative correlation between GDS and Glu+Gln/Cr+PCr in cerebral gray matter (r=0.643, p=0.003).

There was a positive correlation between the STROOP scores and NAA+NAAG/Cr+PCr in precuneus (r=0.476, p=0.039). The test score of line orientation had a positive correlation with Glu+Gln/Cr+PCr in precuneus (r=0.472, p=0.041) and mI/Cr+PCr in frontal lobe (r=0.536, p=0.018). Additionally, SDMT had a positive correlation with Glu+Gln/Cr+PCr in occipital lobe (r=0.537, p=0.018) and NAA+NAAG/Cr+PCr in posterior cingulate gyrus (r=0.572, p=0.011). There were not any significant correlations between UPDRS test scores and the metabolite ratios

in seven different regions.

3.4 Spatial Distribution of ^{1}H-MRSI

Glu+Gln, Cho, mI and NAA+NAAG to Cr+PCr metabolite ratios were compared between PD-MCI and PD-CN and reported in section 3.2. In addition, spatial distribution of ^{1}H-MRSI peaks in patients with Parkinson's disease with mild cognitive impairment (PD-MCI) or cognitively normal (PD-CN) were assessed to define regional spectroscopic differences. Friedman statistic test was used to test for differences among seven different regions including precuneus, occipital lobe, posterior cingulate gyrus, white matter, thalamus, frontal lobe and cerebral gray matter.

Table 3.6 shows mean rank of metabolite ratios in PD-CN in these regions. P values of each group was smaller than 0.01. That is, there were statistically significant differences among these regions for both PD-MCI and PD-CN. Glu+Gln/Cr+PCr was significantly different between occipital lobe and cerebral gray matter. Cho/Cr+PCr of white matter and thalamus had significantly different values than precuneus, occipital lobe, and posterior cingulate gyrus. NAA+NAAG/Cr+PCr in precuneus and posterior cingulate gyrus were significantly different. NAA+NAAG/Cr+PCr of posterior cingulate gyrus and cerebral gray matter were significantly different than thalamus. mI/Cr+PCr was similar in all regions of interest.

Table 3.7 displays the mean rank of metabolite ratios in PD-MCI. The spatial distributions of Cho/Cr+PCr and NAA+NAAG/Cr+PCr were different among different regions. However, there was not any difference in Glu+Gln/Cr+PCr, and mI /Cr+PCr. After Friedman statistics, SNK post-hoc test was applied to determine where the specific differences lie. Cho/Cr+PCr of cerebral white matter, thalamus, and frontal were significantly different from occipital and posterior cingulate gyrus. Cho/Cr+PCr in precuneus and thalamus were significantly different. NAA+NAAG/ Cr+PCr of occipital lobe, white matter, and thalamus were significantly different from posterior cingulate gyrus and cerebral gray matter. NAA+NAAG/Cr+PCr of poste-

rior cingulate gyrus, and cerebral gray matter were significantly different from cerebral white matter and thalamus.

Table 3.4
Spearman's correlation between metabolite ratios and neuropsychological test scores for PD-CN.

			ACE-R		GDS		UPDRS		STROOP		Line		SDMT	
PD-CN		Mean±std	r	p	r	p	r	p	r	p	r	p	r	p
Precuneus	Glu+Gln/(Cr+PCr)	2.42±2.08	0.04	0.87	0.24	0.30	0.06	0.80	-0.12	0.59	-0.09	0.67	0.09	0.71
	Cho/(Cr+PCr)	0.26±0.05	0.06	0.79	0.08	0.73	-0.24	0.29	0.25	0.27	0.09	0.69	0.21	0.37
	mI/(Cr+PCr)	1.18±0.63	0.32	0.15	0.10	0.67	-0.14	0.54	0.04	0.87	-0.01	0.95	0.06	0.79
	NAA+NAAG/(Cr+PCr)	1.53±0.24	0.01	0.96	-0.01	0.96	0.12	0.61	-0.12	0.59	-0.01	0.96	0.01	0.95
Occipital Lobe	Glu+Gln/(Cr+PCr)	1.42±0.33	-0.04	0.84	-0.25	0.26	0.11	0.63	0.05	0.83	0.05	0.84	0.08	0.73
	Cho/(Cr+PCr)	0.25±0.05	-0.10	0.65	0.36	0.11	0.25	0.28	-0.13	0.56	-0.19	0.41	0.13	0.56
	mI/(Cr+PCr)	1.23±0.96	0.11	0.65	0.43	0.05	-0.06	0.77	-0.12	0.59	-0.02	0.92	0.31	0.17
	NAA+NAAG/(Cr+PCr)	1.49±0.21	0.17	0.45	-0.20	0.37	0.13	0.57	0.00	1.00	0.34	0.14	0.16	0.48
Posterior Cingulate Gyrus	Glu+Gln/(Cr+PCr)	1.92±0.93	-0.14	0.54	0.28	0.22	0.35	0.12	0.07	0.75	-0.23	0.31	0.07	0.76
	Cho/(Cr+PCr)	0.27±0.04	-0.20	0.38	0.30	0.19	-0.009	0.97	0.28	0.22	-0.45	0.04*	0.49	0.02*
	mI/(Cr+PCr)	0.73±0.23	-0.26	0.24	0.23	0.33	-0.25	0.26	-0.10	0.67	-0.65	0.001**	0.17	0.46
	NAA+NAAG/(Cr+PCr)	1.26±0.12	0.07	0.76	0.02	0.95	-0.26	0.24	-0.03	0.89	0.36	0.11	0.17	0.46
Cerebral White Matter	Glu+Gln/(Cr+PCr)	1.71±0.93	-0.40	0.07	0.21	0.37	0.43	0.05	0.07	0.78	-0.41	0.06	0.40	0.07
	Cho/(Cr+PCr)	0.33±0.05	0.06	0.79	-0.08	0.71	-0.22	0.32	0.32	0.16	-0.12	0.60	0.04	0.86
	mI/(Cr+PCr)	0.79±0.39	-0.18	0.42	0.14	0.55	-0.13	0.56	0.06	0.80	-0.44	0.05	0.32	0.16
	NAA+NAAG/(Cr+PCr)	1.37±0.19	0.03	0.90	-0.37	0.09	-0.08	0.71	0.31	0.17	0.28	0.22	0.03	0.88
Thalamus	Glu+Gln/(Cr+PCr)	2.27±1.84	0.10	0.66	0.28	0.21	0.00	0.99	0.23	0.32	0.13	0.58	0.01	0.97
	Cho/(Cr+PCr)	0.44±0.23	0.04	0.88	-0.001	1.00	0.38	0.09	-0.04	0.84	-0.04	0.84	0.32	0.16
	mI/(Cr+PCr)	1.25±0.80	-0.27	0.23	0.15	0.52	0.25	0.29	0.15	0.53	0.25	0.28	0.27	0.24
	NAA+NAAG/(Cr+PCr)	1.77±0.67	0.03	0.88	-0.43	0.04*	-0.05	0.80	-0.06	0.79	-0.00	0.99	0.04	0.85
Frontal Lobe	Glu+Gln/(Cr+PCr)	2.61±2.32	-0.04	0.86	-0.17	0.46	0.11	0.63	-0.22	0.33	0.09	0.70	0.08	0.73
	Cho/(Cr+PCr)	0.30±0.04	-0.40	0.07	0.25	0.27	-0.18	0.43	0.23	0.31	-0.34	0.13	0.31	0.18
	mI/(Cr+PCr)	1.14±0.69	-0.1	0.42	-0.26	0.25	-0.02	0.92	0.07	0.78	-0.30	0.18	0.01	0.98
	NAA+NAAG/(Cr+PCr)	1.38±0.30	0.26	0.26	-0.37	0.09	0.00	0.99	0.40	0.08	0.31	0.17	0.09	0.71
Cerebral Gray Matter	Glu+Gln/(Cr+PCr)	2.53±2.00	-0.07	0.76	-0.04	0.83	0.18	0.43	-0.11	0.62	-0.11	0.61	0.06	0.79
	Cho/(Cr+PCr)	0.31±0.07	-0.14	0.53	0.03	0.90	-0.01	0.94	0.11	0.65	-0.36	0.10	0.06	0.79
	mI/(Cr+PCr)	1.06±0.58	0.25	0.28	-0.11	0.63	0.12	0.62	0.19	0.40	-0.28	0.22	0.02	0.92
	NAA+NAAG/(Cr+PCr)	1.49±0.63	0.08	0.72	-0.27	0.23	0.13	0.58	0.31	0.17	0.03	0.89	0.10	0.66

(*p<0.05, **p<0.002)

Table 3.5
Spearman's correlation between metabolite ratios and neuropsychological test scores for PD-MCI.

			ACE-R		GDS		UPDRS		STROOP		Line		SDMT	
PD-MCI		Mean±std	r	p	r	p	r	p	r	p	r	p	r	p
Precuneus	Glu+Gln/(Cr+PCr)	2.49±1.83	-0.33	0.16	0.43	0.07	0.06	0.80	-0.005	0.98	0.47	0.04*	0.01	0.97
	Cho/(Cr+PCr)	0.27±0.05	-0.34	0.15	0.03	0.91	0.27	0.26	-0.14	0.55	- 0.06	0.78	0.09	0.70
	mI/(Cr+PCr)	1.53±0.80	-0.13	0.57	0.07	0.79	0.43	0.07	-0.14	0.57	-0.03	0.90	0.08	0.74
	NAA+NAAG/(Cr+PCr)	1.44±0.31	0.04	0.86	0.13	0.59	0.36	0.13	0.48	0.03*	-0.03	0.90	0.01	0.97
Occipital Lobe	Glu+Gln/(Cr+PCr)	1.65±0.67	0.3	0.21	0.28	0.25	0.14	0.57	0.27	0.27	0.37	0.12	0.54	0.01*
	Cho/(Cr+PCr)	0.25±0.05	-0.26	0.27	0.10	0.69	0.05	0.85	-0.31	0.18	0.11	0.65	-0.03	0.90
	mI/(Cr+PCr)	2.39±4.15	0.11	0.98	0.14	0.57	-0.04	0.87	-0.20	0.41	0.17	0.48	0.27	0.27
	NAA+NAAG/(Cr+PCr)	1.66±0.54	0.08	0.73	-0.44	0.05	-0.61	0.01*	-0.15	0.54	0.33	0.17	0.41	0.08
Posterior Cingulate Gyrus	Glu+Gln/(Cr+PCr)	2.23±1.22	-0.08	0.74	0.08	0.76	-0.16	0.49	-0.09	0.70	-0.23	0.33	-0.29	0.23
	Cho/(Cr+PCr)	0.27±0.04	0.15	0.53	0.33	0.17	0.33	0.18	-0.11	0.63	-0.12	0.63	-0.01	0.94
	mI/(Cr+PCr)	0.95±0.54	0.15	0.54	0.05	0.84	-0.02	0.93	-0.21	0.39	0.10	0.68	0.03	0.92
	NAA+NAAG/(Cr+PCr)	1.26±0.17	0.53	0.01*	-0.22	0.37	-0.45	0.05	-0.27	0.26	0.20	0.42	0.57	0.01*
Cerebral White Matter	Glu+Gln/(Cr+PCr)	2.16±1.74	-0.18	0.44	0.13	0.60	0.31	0.20	-0.03	0.88	-0.22	0.35	-0.26	0.27
	Cho/(Cr+PCr)	0.63±1.31	-0.40	0.09	-0.09	0.69	0.10	0.68	-0.41	0.08	-0.30	0.21	-0.37	0.11
	mI/(Cr+PCr)	1.34±1.25	-0.14	0.56	-0.06	0.80	0.00	0.99	-0.09	0.69	-0.41	0.08	0.41	0.08
	NAA+NAAG/(Cr+PCr)	1.77±1.29	0.16	0.51	-0.27	0.25	-0.37	0.11	-0.38	0.10	-0.18	0.44	0.10	0.69
Thalamus	Glu+Gln/(Cr+PCr)	3.03±3.06	-0.35	0.14	-0.09	0.71	0.01	0.97	-0.12	0.62	0.09	0.73	-0.21	0.37
	Cho/(Cr+PCr)	0.37±0.10	0.01	0.96	-0.105	0.67	-0.20	0.41	0.08	0.74	0.04	0.86	-0.01	0.94
	mI/(Cr+PCr)	1.44±0.85	-0.27	0.25	0.23	0.33	-0.01	0.96	0.01	0.97	-0.14	0.56	-0.23	0.32
	NAA+NAAG/(Cr+PCr)	1.77±0.60	0.1	0.67	-0.29	0.23	-0.33	0.16	-0.007	0.98	0.03	0.90	0.04	0.89
Frontal Lobe	Glu+Gln/(Cr+PCr)	3.63±5.70	-0.29	0.23	-0.24	0.30	0.14	0.56	-0.42	0.07	-0.11	0.64	-0.13	0.59
	Cho/(Cr+PCr)	0.34±0.07	0.05	0.81	0.29	0.23	0.43	0.06	-0.17	0.48	-0.001	1.00	-0.04	0.87
	mI/(Cr+PCr)	1.29±0.60	-0.14	0.56	0.40	0.10	-0.004	0.99	-0.34	0.15	0.54	0.01*	0.04	0.87
	NAA+NAAG/(Cr+PCr)	1.34±0.40	-0.12	0.62	-0.33	0.16	-0.29	0.22	-0.01	0.94	0.28	0.24	0.25	0.30
Cerebral Gray Matter	Glu+Gln/(Cr+PCr)	3.33±7.12	-0.24	0.31	-0.64	0.003*	-0.16	0.50	-0.13	0.59	-0.42	0.07	0.24	0.33
	Cho/(Cr+PCr)	0.32±0.06	0.28	0.24	-0.25	0.29	0.00	1.00	-0.22	0.36	-0.22	0.36	-0.32	0.17
	mI/(Cr+PCr)	1.78±2.61	-0.29	0.22	0.05	0.84	0.06	0.81	-0.43	0.06	0.19	0.44	-0.18	0.45
	NAA+NAAG/(Cr+PCr)	1.17±0.24	0.12	0.62	0.08	0.74	0.35	0.15	0.25	0.31	-0.05	0.84	0.05	0.85

(*p<0.05, **p<0.002)

Table 3.6
Spatial distribution of metabolite ratios of patients with PD-CN in different regions.

	Precuneus	Occipital Lobe	Posterior Cingulate Gyrus	Cerebral White Matter	Thalamus	Frontal Lobe	Cerebral Gray Matter	p
Glu+Gln/(Cr+PCr)	4.40	2.74	4.29	2.95	4.05	4.60	4.98	0.004
Cho/(Cr+PCr)	2.98	2.45	2.81	5.24	6.00	4.17	4.36	<.001*
mI/(Cr+PCr)	4.69	4.26	2.76	3.05	4.67	4.31	4.26	0.013
NAA+NAAG/(Cr+PCr)	5.07	4.40	2.52	3.86	5.24	3.64	3.26	<.001*

(*p<0.01)

Table 3.7
Spatial distribution of metabolite ratios of patients with PD-MCI in different regions.

	Precuneus	Occipital Lobe	Posterior Cingulate Gyrus	Cerebral White Matter	Thalamus	Frontal Lobe	Cerebral Gray Matter	p
Glu+Gln/(Cr+PCr)	4.58	3.11	4.50	3.42	4.00	4.89	3.50	0.08
Cho/(Cr+PCr)	3.11	2.32	2.92	5.00	5.32	5.00	4.34	<.001*
mI/(Cr+PCr)	4.68	4.00	2.76	3.79	4.42	4.32	4.03	0.15
NAA+NAAG/(Cr+PCr)	4.16	5.26	2.55	4.74	5.37	3.79	2.13	<.001*

(*p<0.01)

4. DISCUSSION

The aim of this study was to determine a biomarker that indicates the presence of PD-MCI in comparison to PD-CN. We developed a novel MRSI data analysis tool that automatically registered metabolite maps obtained from LCModel onto MNI152 brain atlas.

3D ^{1}H-MRSI data analysis usually depends on visual definition of regions of interest, because this approach requires minimum expertise in analysis. It is especially useful when there is not any data analysis software tools available. However, this approach requires a basic knowledge of anatomy. Additionally, a wider region in the brain such as whole frontal lobe could be easily delineated, but locating small parts of the brain like thalamus could prove difficult. As a result, this common approach might result in biased results. Many software packages such as FSL, SPM, and AFNI provide superior atlas based ROI analysis that has been commonly employed for fMRI, MRI, and DTI [77, 78]. However, there has not any studies about atlas based registration of MRSI metabolite maps overlaid onto reference T2-weighted MR images, which has been accomplished in our study. Compared to visual definition of ROIs, FSL atlas toolbox was very easy to use, and resulted in a more accurate definition of ROIs even if the region was small. This systematic approach would reduce the differences between the studies. Additionally, registering MRSI data to MNI 152 brain atlas and using unbiased FSL atlas toolbox to define the ROIs would enable us to apply group analysis once all the data are registered onto the atlas.

There has been a previous study that registered T2-weighted images to MNI152 brain atlas in order to locate a single voxel automatically during scan to reduce operator dependent bias in voxel selection [79]. However, they did not use three dimensional MRSI maps by registering to MNI152 atlas, which was completed in this study that will have a significant impact on MRSI data analysis.

Summerfield et al. and Griffith et al. reported that low NAA/Cr in occipital lobe might be an indicator of PDD [69, 73, 80]. These studies were performed with 3 groups, which were healthy control, PD-CN, and PDD. A few years later, Nie et al. [74] observed a reduction of NAA/Cr in patients with PD-MCI compared with PD-CN and healthy controls. This results are in agreement that reduced NAA/Cr may be a marker of PD-MCI and PDD. However, we did not observe a reduction of NAA/Cr in occipital lobe in PD-MCI. Posterior cingulate gyrus was another region under focus. Lower NAA/Cr level in posterior cingulate gyrus was observed in PDD, and in PD with non-demented mild to moderately according to the studies of Camicioli et al. and Almuqbel et al. [70, 75], which isn't in agreement with our findings. While an increased level of Cho in posterior cingulate gyrus was observed in PD-MCI and PDD patients according to findings of Nie et al. [74] and Almuqbel et al. [75], our findings showed that there was not any significant difference between groups.

This inconsistency with previous studies might be due to the number of patients and data acquisition differences. For instance, Nie et al. [74] had 3 times bigger patient population than us, and they included 66 patients with PD-MCI, 70 patients with PD-CN, and 74 healthy controls. The second difference that creates inconsistent result is data acquisition differences. While previous studies preferred single voxel MRS to obtain the data, multi voxel MRSI was performed in our study to scan wider regions, which might have resulted in peak ratio differences at the same region.

We have observed a trend for a higher Cho/Cr and mI/Cr in frontal lobe and cerebral white matter, which might be important. Even though these regions weren't under focus directly in PD-MCI or PDD before, the results may be relatable to Alzheimer MCI studies. Increased mI/Cr was identified as an early biomarker that shows a progression of a patient from CN to MCI in the course of AD [71]. Increased Cho/Cr+PCr was previously associated with MCI and thought to be a marker of progression from AD to AD-MCI [81].

Correlations between metabolite ratios and neuropsychological tests provide severity important aspects of view. There is a statistically negative correlation be-

tween mI/Cr+PCr and line orientation in posterior cingulate. This might make sense, since increased mI may be related to AD, gliosis, and demyelination. There was trend for a negative correlation between NAA+NAAG/Cr+PCr and GDS test score in thalamus, because decreased NAA level shows a neuronal dysfunction. A trend for a positive correlation between NAA+NAAG/Cr+PCr and ACE-R test score in occipital lobe makes sense, because lower ACE-R score may be related to low cognitive functions. Since increased Cho level may be a biomarker of progression of AD, ischemia, acute brain injury and cancer, a negative correlation between line orientation test and Cho/Cr+PCr in posterior cingulate gyrus might be possible. There was trend for a positive correlation between NAA+NAAG/Cr+PCr and SDMT test score, because we expect a patient with cognitive dysfunction get a lower SDMT score.

The present study has several limitations. There were only two groups, which were PD-MCI and PD-CN. There weren't any healthy controls involved in this study. Therefore, we didn't compare the differences among all three groups for more reliable results. The number of participants was another limitation of this study.

5. CONCLUSION

The main aim of this study was to develop an MRSI data analysis tool and find a possible biomarker for PD-MCI. This was the first study in the literature that enabled the assessment of the results of ^{1}H-MRSI by registering ^{1}H MR spectroscopic peak parameter maps overlaid onto reference T2-weighted MR images to MNI152 brain atlas. Future studies will investigate MR spectroscopic changes in a higher number of patients, and will include healthy controls. The data acquisition will be repeated after 1.5 years, and a longitudinal study of MRSI of PD-MCI will be conducted. Additionally, we plan to combine our results with other MR scan techniques' results to create a multimodality brain map of PD-MCI.

APPENDIX A. Software Packages

1. FSL (http://fsl.fmrib.ox.ac.uk/fsl/fslwiki/),

2. MATLAB (http://www.mathworks.com/downloads/).

REFERENCES

1. Smith, S. M., M. Jenkinson, M. W. Woolrich, C. F. Beckmann, T. E. Behrens, H. Johansen-Berg, P. R. Bannister, M. De Luca, I. Drobnjak, D. E. Flitney, R. K. Niazy, J. Saunders, J. Vickers, Y. Zhang, N. De Stefano, J. M. Brady, and P. M. Matthews, "Advances in functional and structural mr image analysis and implementation as fsl," *Neuroimage*, Vol. 23 Suppl 1, pp. S208–19, 2004.

2. Smith, S. M., "Fast robust automated brain extraction," *Hum Brain Mapp*, Vol. 17, no. 3, pp. 143–55, 2002.

3. Jenkinson, M., and S. Smith, "A global optimisation method for robust affine registration of brain images," *Med Image Anal*, Vol. 5, no. 2, pp. 143–56, 2001.

4. Davatzikos, C., J. L. Prince, and R. N. Bryan, "Image registration based on boundary mapping," *IEEE Trans Med Imaging*, Vol. 15, no. 1, pp. 112–5, 1996.

5. Ozturk-Isik, E., J. C. Crane, S. Cha, S. M. Chang, M. S. Berger, and S. J. Nelson, "Unaliasing lipid contamination for mr spectroscopic imaging of gliomas at 3t using sensitivity encoding (sense)," *Magn Reson Med*, Vol. 55, no. 5, pp. 1164–9, 2006.

6. Ross, B., and S. Bluml, "Magnetic resonance spectroscopy of the human brain," *Anat Rec*, Vol. 265, no. 2, pp. 54–84, 2001.

7. Kelm, B. M., F. O. Kaster, A. Henning, M. A. Weber, P. Bachert, P. Boesiger, F. A. Hamprecht, and B. H. Menze, "Using spatial prior knowledge in the spectral fitting of mrs images," *NMR Biomed*, Vol. 25, no. 1, pp. 1–13, 2012.

8. Croitor Sava, A. R., D. M. Sima, J. B. Poullet, A. J. Wright, A. Heerschap, and S. Van Huffel, "Exploiting spatial information to estimate metabolite levels in two-dimensional mrsi of heterogeneous brain lesions," *NMR Biomed*, Vol. 24, no. 7, pp. 824–35, 2011.

9. Riddle, W. R., S. J. Gibbs, and M. R. Willcott, "Dissecting and implementing steam spectroscopy," *Magn Reson Med*, Vol. 29, no. 3, pp. 378–80, 1993.

10. Provencher, S. W., "Estimation of metabolite concentrations from localized in vivo proton nmr spectra," *Magn Reson Med*, Vol. 30, no. 6, pp. 672–9, 1993.

11. Provencher, S. W., "Automatic quantitation of localized in vivo 1h spectra with lcmodel," *NMR Biomed*, Vol. 14, no. 4, pp. 260–4, 2001.

12. Mandal, P. K., "In vivo proton magnetic resonance spectroscopic signal processing for the absolute quantitation of brain metabolites," *Eur J Radiol*, Vol. 81, no. 4, pp. e653–64, 2012.

13. Naressi, A., C. Couturier, I. Castang, R. de Beer, and D. Graveron-Demilly, "Java-based graphical user interface for mrui, a software package for quantitation of in vivo/medical magnetic resonance spectroscopy signals," *Comput Biol Med*, Vol. 31, no. 4, pp. 269–86, 2001.

14. Mullins, P. G., L. Rowland, J. Bustillo, E. J. Bedrick, J. Lauriello, and W. M. Brooks, "Reproducibility of 1h-mrs measurements in schizophrenic patients," *Magn Reson Med*, Vol. 50, no. 4, pp. 704–7, 2003.

15. O'Gorman, R. L., L. Michels, R. A. Edden, J. B. Murdoch, and E. Martin, "In vivo detection of gaba and glutamate with mega-press: reproducibility and gender effects," *J Magn Reson Imaging*, Vol. 33, no. 5, pp. 1262–7, 2011.

16. Kanowski, M., J. Kaufmann, J. Braun, J. Bernarding, and C. Tempelmann, "Quantitation of simulated short echo time 1h human brain spectra by lcmodel and amares," *Magn Reson Med*, Vol. 51, no. 5, pp. 904–12, 2004.

17. Weis, J., L. Johansson, F. Ortiz-Nieto, and H. Ahlstrom, "Assessment of lipids in skeletal muscle by lcmodel and amares," *J Magn Reson Imaging*, Vol. 30, no. 5, pp. 1124–9, 2009.

18. Vanhamme, L., A. van den Boogaart, and S. Van Huffel, "Improved method for accurate and efficient quantification of mrs data with use of prior knowledge," *J Magn Reson*, Vol. 129, no. 1, pp. 35–43, 1997.

19. Williamson, D. C., H. Hawesa, N. A. Thacker, and S. R. Williams, "Robust quantification of short echo time 1h magnetic resonance spectra using the pade approximant," *Magn Reson Med*, Vol. 55, no. 4, pp. 762–71, 2006.

20. Govindaraju, V., K. Young, and A. A. Maudsley, "Proton nmr chemical shifts and coupling constants for brain metabolites," *NMR Biomed*, Vol. 13, no. 3, pp. 129–53, 2000.

21. Pfeuffer, J., I. Tkac, S. W. Provencher, and R. Gruetter, "Toward an in vivo neurochemical profile: quantification of 18 metabolites in short-echo-time (1)h nmr spectra of the rat brain," *J Magn Reson*, Vol. 141, no. 1, pp. 104–20, 1999.

22. Oz, G., M. Terpstra, I. Tkac, P. Aia, J. Lowary, P. J. Tuite, and R. Gruetter, "Proton mrs of the unilateral substantia nigra in the human brain at 4 tesla: detection of high gaba concentrations," *Magn Reson Med*, Vol. 55, no. 2, pp. 296–301, 2006.

23. Brambilla, P., J. Perez, F. Barale, G. Schettini, and J. C. Soares, "Gabaergic dysfunction in mood disorders," *Mol Psychiatry*, Vol. 8, no. 8, pp. 721–37, 715, 2003.

24. Sanacora, G., G. F. Mason, D. L. Rothman, K. L. Behar, F. Hyder, O. A. Petroff, R. M. Berman, D. S. Charney, and J. H. Krystal, "Reduced cortical gamma-aminobutyric acid levels in depressed patients determined by proton magnetic resonance spectroscopy," *Arch Gen Psychiatry*, Vol. 56, no. 11, pp. 1043–7, 1999.

25. Sanacora, G., R. Gueorguieva, C. N. Epperson, Y. T. Wu, M. Appel, D. L. Rothman, J. H. Krystal, and G. F. Mason, "Subtype-specific alterations of gamma-aminobutyric acid and glutamate in patients with major depression," *Arch Gen Psychiatry*, Vol. 61, no. 7, pp. 705–13, 2004.

26. Petroff, O. A., F. Hyder, D. L. Rothman, and R. H. Mattson, "Homocarnosine and seizure control in juvenile myoclonic epilepsy and complex partial seizures," *Neurology*, Vol. 56, no. 6, pp. 709–15, 2001.

27. Goddard, A. W., G. F. Mason, A. Almai, D. L. Rothman, K. L. Behar, O. A. Petroff, D. S. Charney, and J. H. Krystal, "Reductions in occipital cortex gaba levels in panic disorder detected with 1h-magnetic resonance spectroscopy," *Arch Gen Psychiatry*, Vol. 58, no. 6, pp. 556–61, 2001.

28. Wallimann, T., M. Wyss, D. Brdiczka, K. Nicolay, and H. M. Eppenberger, "Intracellular compartmentation, structure and function of creatine kinase isoenzymes in tissues with high and fluctuating energy demands: the 'phosphocreatine circuit' for cellular energy homeostasis," *Biochem J*, Vol. 281 (Pt 1), pp. 21–40, 1992.

29. Tan, J., S. Bluml, T. Hoang, D. Dubowitz, G. Mevenkamp, and B. Ross, "Lack of effect of oral choline supplement on the concentrations of choline metabolites in human brain," *Magn Reson Med*, Vol. 39, no. 6, pp. 1005–10, 1998.

30. Wang, Y., and S. J. Li, "Differentiation of metabolic concentrations between gray matter and white matter of human brain by in vivo 1h magnetic resonance spectroscopy," *Magn Reson Med*, Vol. 39, no. 1, pp. 28–33, 1998.

31. Pouwels, P. J., and J. Frahm, "Regional metabolite concentrations in human brain as determined by quantitative localized proton mrs," *Magn Reson Med*, Vol. 39, no. 1, pp. 53–60, 1998.

32. Keltner, J. R., L. L. Wald, P. J. Ledden, Y. C. Chen, R. T. Matthews, E. H. Kuestermann, J. R. Baker, B. R. Rosen, and B. G. Jenkins, "A localized double-quantum filter for the in vivo detection of brain glucose," *Magn Reson Med*, Vol. 39, no. 4, pp. 651–6, 1998.

33. de Graaf, R. A., R. M. Dijkhuizen, G. J. Biessels, K. P. Braun, and K. Nicolay, "In vivo glucose detection by homonuclear spectral editing," *Magn Reson Med*, Vol. 43, no. 5, pp. 621–6, 2000.

34. Pan, J. W., G. F. Mason, G. M. Pohost, and H. P. Hetherington, "Spectroscopic imaging of human brain glutamate by water-suppressed j-refocused coherence transfer at 4.1 t," *Magn Reson Med*, Vol. 36, no. 1, pp. 7–12, 1996.

35. Pan, J. W., T. Venkatraman, K. Vives, and D. D. Spencer, "Quantitative glutamate spectroscopic imaging of the human hippocampus," *NMR Biomed*, Vol. 19, no. 2, pp. 209–16, 2006.

36. Tkac, I., P. Andersen, G. Adriany, H. Merkle, K. Ugurbil, and R. Gruetter, "In vivo 1h nmr spectroscopy of the human brain at 7 t," *Magn Reson Med*, Vol. 46, no. 3, pp. 451–6, 2001.

37. Ross, B. D., "Biochemical considerations in 1h spectroscopy. glutamate and glutamine; myo-inositol and related metabolites," *NMR Biomed*, Vol. 4, no. 2, pp. 59–63, 1991.

38. Sian, J., D. T. Dexter, A. J. Lees, S. Daniel, Y. Agid, F. Javoy-Agid, P. Jenner, and C. D. Marsden, "Alterations in glutathione levels in parkinson's disease and other neurodegenerative disorders affecting basal ganglia," *Ann Neurol*, Vol. 36, no. 3, pp. 348–55, 1994.

39. Cooper, A. J., and B. S. Kristal, "Multiple roles of glutathione in the central nervous system," *Biol Chem*, Vol. 378, no. 8, pp. 793–802, 1997.

40. Terpstra, M., T. J. Vaughan, K. Ugurbil, K. O. Lim, S. C. Schulz, and R. Gruetter, "Validation of glutathione quantitation from steam spectra against edited 1h nmr spectroscopy at 4t: application to schizophrenia," *MAGMA*, Vol. 18, no. 5, pp. 276–82, 2005.

41. Bruhn, H., J. Frahm, M. L. Gyngell, K. D. Merboldt, W. Hanicke, R. Sauter, and C. Hamburger, "Noninvasive differentiation of tumors with use of localized h-1 mr spectroscopy in vivo: initial experience in patients with cerebral tumors," *Radiology*, Vol. 172, no. 2, pp. 541–8, 1989.

42. Majos, C., M. Julia-Sape, J. Alonso, M. Serrallonga, C. Aguilera, J. J. Acebes, C. Arus, and J. Gili, "Brain tumor classification by proton mr spectroscopy: comparison of diagnostic accuracy at short and long te," *AJNR Am J Neuroradiol*, Vol. 25, no. 10, pp. 1696–704, 2004.

43. Gideon, P., O. Henriksen, B. Sperling, P. Christiansen, T. S. Olsen, H. S. Jorgensen, and P. Arlien-Soborg, "Early time course of n-acetylaspartate, creatine and phosphocreatine, and compounds containing choline in the brain after acute stroke. a proton magnetic resonance spectroscopy study," *Stroke*, Vol. 23, no. 11, pp. 1566–72, 1992.

44. Bruhn, H., J. Frahm, M. L. Gyngell, K. D. Merboldt, W. Hanicke, and R. Sauter, "Cerebral metabolism in man after acute stroke: new observations using localized proton nmr spectroscopy," *Magn Reson Med*, Vol. 9, no. 1, pp. 126–31, 1989.

45. Arnold, D. L., P. M. Matthews, G. Francis, and J. Antel, "Proton magnetic resonance spectroscopy of human brain in vivo in the evaluation of multiple sclerosis: assessment of the load of disease," *Magn Reson Med*, Vol. 14, no. 1, pp. 154–9, 1990.

46. Larsson, H. B., P. Christiansen, M. Jensen, J. Frederiksen, A. Heltberg, J. Olesen, and O. Henriksen, "Localized in vivo proton spectroscopy in the brain of patients with multiple sclerosis," *Magn Reson Med*, Vol. 22, no. 1, pp. 23–31, 1991.

47. Michaelis, T., G. Helms, K. D. Merboldt, W. Hanicke, H. Bruhn, and J. Frahm, "Identification of scyllo-inositol in proton nmr spectra of human brain in vivo," *NMR Biomed*, Vol. 6, no. 1, pp. 105–9, 1993.

48. Viola, A., F. Nicoli, B. Denis, S. Confort-Gouny, Y. Le Fur, J. P. Ranjeva, P. Viout, and P. J. Cozzone, "High cerebral scyllo-inositol: a new marker of brain metabolism disturbances induced by chronic alcoholism," *MAGMA*, Vol. 17, no. 1, pp. 47–61, 2004.

49. Hardy, D. L., and T. J. Norwood, "Spectral editing technique for the in vitro and in vivo detection of taurine," *J Magn Reson*, Vol. 133, no. 1, pp. 70–8, 1998.

50. Parkinson, J., "An essay on the shaking palsy. 1817," *J Neuropsychiatry Clin Neurosci*, Vol. 14, no. 2, pp. 223–36; discussion 222, 2002.

51. Dorsey, E. R., R. Constantinescu, J. P. Thompson, K. M. Biglan, R. G. Holloway, K. Kieburtz, F. J. Marshall, B. M. Ravina, G. Schifitto, A. Siderowf, and C. M. Tanner, "Projected number of people with parkinson disease in the most populous nations, 2005 through 2030," *Neurology*, Vol. 68, no. 5, pp. 384–6, 2007.

52. Baba, M., S. Nakajo, P. H. Tu, T. Tomita, K. Nakaya, V. M. Lee, J. Q. Trojanowski, and T. Iwatsubo, "Aggregation of alpha-synuclein in lewy bodies of sporadic parkinson's disease and dementia with lewy bodies," *Am J Pathol*, Vol. 152, no. 4, pp. 879–84, 1998.

53. Galvin, J. E., V. M. Lee, and J. Q. Trojanowski, "Synucleinopathies: clinical and pathological implications," *Arch Neurol*, Vol. 58, no. 2, pp. 186–90, 2001.

54. Jankovic, J., "Parkinson's disease: clinical features and diagnosis," *J Neurol Neurosurg Psychiatry*, Vol. 79, no. 4, pp. 368–76, 2008.

55. Petersen, R. C., J. C. Stevens, M. Ganguli, E. G. Tangalos, J. L. Cummings, and S. T. DeKosky, "Practice parameter: early detection of dementia: mild cognitive impairment (an evidence-based review). report of the quality standards subcommittee of the american academy of neurology," *Neurology*, Vol. 56, no. 9, pp. 1133–42, 2001.

56. Aarsland, D., M. K. Beyer, and M. W. Kurz, "Dementia in parkinson's disease," *Curr Opin Neurol*, Vol. 21, no. 6, pp. 676–82, 2008.

57. Petersen, R. C., "Mild cognitive impairment as a diagnostic entity," *J Intern Med*, Vol. 256, no. 3, pp. 183–94, 2004.

58. Mariani, E., R. Monastero, and P. Mecocci, "Mild cognitive impairment: a systematic review," *J Alzheimers Dis*, Vol. 12, no. 1, pp. 23–35, 2007.

59. Forlenza, O. V., B. S. Diniz, P. V. Nunes, C. M. Memoria, M. S. Yassuda, and W. F. Gattaz, "Diagnostic transitions in mild cognitive impairment subtypes," *Int Psychogeriatr*, Vol. 21, no. 6, pp. 1088–95, 2009.

60. Libon, D. J., S. X. Xie, J. Eppig, G. Wicas, M. Lamar, C. Lippa, B. M. Bettcher, C. C. Price, T. Giovannetti, R. Swenson, and D. M. Wambach, "The heterogeneity of mild cognitive impairment: a neuropsychological analysis," *J Int Neuropsychol Soc*, Vol. 16, no. 1, pp. 84–93, 2010.

61. Martinez-Martin, P., A. Gil-Nagel, L. M. Gracia, J. B. Gomez, J. Martinez-Sarries, and F. Bermejo, "Unified parkinson's disease rating scale characteristics and structure. the cooperative multicentric group," *Mov Disord*, Vol. 9, no. 1, pp. 76–83, 1994.

62. Golden, C. J., "A group version of the stroop color and word test," *J Pers Assess*, Vol. 39, no. 4, pp. 386–8, 1975.

63. Gullett, J. M., C. C. Price, P. Nguyen, M. S. Okun, R. M. Bauer, and D. Bowers, "Reliability of three benton judgment of line orientation short forms in idiopathic parkinson's disease," *Clin Neuropsychol*, Vol. 27, no. 7, pp. 1167–78, 2013.

64. Sheridan, L. K., H. E. Fitzgerald, K. M. Adams, J. T. Nigg, M. M. Martel, L. I. Puttler, M. M. Wong, and R. A. Zucker, "Normative symbol digit modalities test performance in a community-based sample," *Arch Clin Neuropsychol*, Vol. 21, no. 1, pp. 23–8, 2006.

65. Monchi, O., M. Petrides, V. Petre, K. Worsley, and A. Dagher, "Wisconsin card sorting revisited: distinct neural circuits participating in different stages of the task identified by event-related functional magnetic resonance imaging," *J Neurosci*, Vol. 21, no. 19, pp. 7733–41, 2001.

66. Litvan, I., J. G. Goldman, A. I. Troster, B. A. Schmand, D. Weintraub, R. C. Petersen, B. Mollenhauer, C. H. Adler, K. Marder, C. H. Williams-Gray, D. Aarsland, J. Kulisevsky, M. C. Rodriguez-Oroz, D. J. Burn, R. A. Barker, and M. Emre, "Diagnostic criteria for mild cognitive impairment in parkinson's disease: Movement disorder society task force guidelines," *Mov Disord*, Vol. 27, no. 3, pp. 349–56, 2012.

67. Aarsland, D., K. Andersen, J. P. Larsen, A. Lolk, and P. Kragh-Sorensen, "Prevalence and characteristics of dementia in parkinson disease: an 8-year prospective study," *Arch Neurol*, Vol. 60, no. 3, pp. 387–92, 2003.

68. Hely, M. A., W. G. Reid, M. A. Adena, G. M. Halliday, and J. G. Morris, "The sydney multicenter study of parkinson's disease: the inevitability of dementia at 20 years," *Mov Disord*, Vol. 23, no. 6, pp. 837–44, 2008.

69. Summerfield, C., B. Gomez-Anson, E. Tolosa, J. M. Mercader, M. J. Marti, P. Pastor, and C. Junque, "Dementia in parkinson disease: a proton magnetic resonance spectroscopy study," *Arch Neurol*, Vol. 59, no. 9, pp. 1415–20, 2002.

70. Camicioli, R. M., J. R. Korzan, S. L. Foster, N. J. Fisher, D. J. Emery, A. C. Bastos, and C. C. Hanstock, "Posterior cingulate metabolic changes occur in parkinson's disease patients without dementia," *Neurosci Lett*, Vol. 354, no. 3, pp. 177–80, 2004.

71. Kantarci, K., G. E. Smith, R. J. Ivnik, R. C. Petersen, B. F. Boeve, D. S. Knopman, E. G. Tangalos, and J. Jack, C. R., "1h magnetic resonance spectroscopy, cognitive function, and apolipoprotein e genotype in normal aging, mild cognitive impairment and alzheimer's disease," *J Int Neuropsychol Soc*, Vol. 8, no. 7, pp. 934–42, 2002.

72. Griffith, H. R., O. C. Okonkwo, T. O'Brien, and J. A. Hollander, "Reduced brain glutamate in patients with parkinson's disease," *NMR Biomed*, Vol. 21, no. 4, pp. 381–7, 2008.

73. Griffith, H. R., J. A. den Hollander, O. C. Okonkwo, T. O'Brien, R. L. Watts, and D. C. Marson, "Brain metabolism differs in alzheimer's disease and parkinson's disease dementia," *Alzheimers Dement*, Vol. 4, no. 6, pp. 421–7, 2008.

74. Nie, K., Y. Zhang, B. Huang, L. Wang, J. Zhao, Z. Huang, R. Gan, and L. Wang, "Marked n-acetylaspartate and choline metabolite changes in parkinson's disease patients with mild cognitive impairment," *Parkinsonism Relat Disord*, Vol. 19, no. 3, pp. 329–34, 2013.

75. Almuqbel, M., T. R. Melzer, D. J. Myall, M. R. MacAskill, T. L. Pitcher, L. Livingston, K. L. Wood, R. J. Keenan, J. C. Dalrymple-Alford, and T. J. Anderson, "Metabolite ratios in the posterior cingulate cortex do not track cognitive decline in parkinson's disease in a clinical setting," *Parkinsonism Relat Disord*, Vol. 22, pp. 54–61, 2016.

76. Hanstock, C., and M. Gee, "Serial magnetic resonance spectroscopy of the human brain - atlas-based automated volume registration with high precision and reproducibility.," 20-26 April 2013 2013.

77. Poldrack, R. A., "Region of interest analysis for fmri," *Soc Cogn Affect Neurosci*, Vol. 2, no. 1, pp. 67–70, 2007.

78. Greve, D. N., and B. Fischl, "Accurate and robust brain image alignment using boundary-based registration," *Neuroimage*, Vol. 48, no. 1, pp. 63–72, 2009.

79. Gong, Y. U., J. Yu, D. Pang, H. Zhen, J. Galvin, and Y. Xiao, "Automated extraction of dose/volume statistics for radiotherapy-treatment-plan evaluation in clinical-trial quality assurance," *Front Oncol*, Vol. 6, p. 47, 2016.

80. Griffith, H. R., J. A. den Hollander, O. C. Okonkwo, T. O'Brien, R. L. Watts, and D. C. Marson, "Brain n-acetylaspartate is reduced in parkinson disease with dementia," *Alzheimer Dis Assoc Disord*, Vol. 22, no. 1, pp. 54–60, 2008.

81. Firbank, M. J., R. M. Harrison, and J. T. O'Brien, "A comprehensive review of proton magnetic resonance spectroscopy studies in dementia and parkinson's disease," *Dement Geriatr Cogn Disord*, Vol. 14, no. 2, pp. 64–76, 2002.